Validation of Thermosphere Ionosphere Mesosphere Energetics and Dynamics/Sounding of the Atmosphere using Broadband Emission Radiometry (TIMED/SABER) v1.07 ozone at 9.6 μm in altitude range 15–70 km

P. P. Rong,[1] J. M. Russell III,[1] M. G. Mlynczak,[2] E. E. Remsberg,[2] B. T. Marshall,[3] L. L. Gordley,[3] and M. López-Puertas[4]

Received 5 March 2008; revised 16 October 2008; accepted 24 November 2008; published 21 February 2009.

[1] The Sounding of the Atmosphere using Broadband Emission Radiometry (SABER) instrument operating onboard the Thermosphere Ionosphere Mesosphere Energetics and Dynamics (TIMED) satellite since 2002 has provided day and nighttime measurements of ozone on a daily basis in the middle to upper atmosphere (15–100 km) using limb scanning in the 9.6-μm band. The focus of this paper is on validation of v1.07 O_3 in the stratosphere and mesosphere region below 70 km. SABER v1.07 O_3 measurements have a precision of ~1–2% in the stratosphere and ~3–5% in the lower mesosphere. A SABER positive bias exists in all regions other than the lower stratosphere. The positive biases in the stratosphere are within ~5–12% in most cases except in the equatorial to middle latitudes in the altitude range ~30–50 km, where they reach ~15–17% and exceed the combined systematic error by ~5–6%. The comparisons in the lower mesosphere indicate that SABER O_3 captures the diurnal variability very well. The best agreement of ~5–7% occurs for daytime comparisons with solar occultation measurements in the lower mesosphere. As with most large satellite data sets, a small portion of the O_3 profiles show unrealistically large values. The occurrences of these profiles were revealed using a probability approach, which enabled the identification of the time frames and spatial regions where these anomalies occur.

Citation: Rong, P. P., J. M. Russell III, M. G. Mlynczak, E. E. Remsberg, B. T. Marshall, L. L. Gordley, and M. López-Puertas (2009), Validation of Thermosphere Ionosphere Mesosphere Energetics and Dynamics/Sounding of the Atmosphere using Broadband Emission Radiometry (TIMED/SABER) v1.07 ozone at 9.6 μm in altitude range 15–70 km, *J. Geophys. Res.*, *114*, D04306, doi:10.1029/2008JD010073.

1. Introduction

[2] Ozone plays an important role in the radiative balance of the Earth's atmosphere and it is vital to life on Earth. It is a key participant in the photochemistry of the middle to upper atmosphere. Concern about the integrity of the ozone layer has existed for many years because of the annual occurrence of the Antarctic ozone hole or spring minimum in the stratosphere that has been shown to result from human use of chlorofluoromethanes. Recent findings since 2004 also suggest that short-term stratospheric ozone loss can occur because of upper atmospheric connections and may be linked to solar activity. For example, the unprecedented ozone loss throughout the lower mesosphere and upper stratosphere in the 2004 and 2006 springs, in association with the strong nitric oxide descent during the winter time in both years, attracted much attention and led to a series of research papers [e.g., *Seppälä et al.*, 2004; *Randall et al.*, 2005, 2006]. Long-term ozone measurements at high altitudes (e.g., mesosphere and lower thermosphere, or MLT region) and with global coverage will lead to better understanding of these occurrences.

[3] A number of satellite missions have been launched within the last 7 years to measure ozone and other parameters including, for example, POES/SBUV/2 (solar backscatter ultraviolet) [*Bhartia et al.*, 1996], ENVISAT/MIPAS (Michelson Interferometer for Passive Atmospheric Sounding) from ESA (European Space Agency) [*Fischer et al.*, 2000], AURA/MLS (Microwave Limb Sounder) [*Waters et al.*, 2006], AURA/HIRDLS (High Resolution Dynamics Limb Sounder) [*Dials et al.*, 1998], and TIMED/SABER (Sounding of the Atmosphere Using Broadband Emission Radiometry) [*Russell et al.*, 1999] from NASA. Obtaining data at altitudes above 50 km is either marginal for most of these missions because it is near their upper limit of vertical coverage, or the vertical resolution is somewhat coarse (6–7 km). SABER/TIMED was designed for high-altitude sounding and near-global coverage. SABER noise

[1] Hampton University, Hampton, Virginia, USA.
[2] NASA Langley Research Center, Hampton, Virginia, USA.
[3] GATS, Inc., Newport News, Virginia, USA.
[4] Instituto de Astrofísica de Andalucíca, CSIC, Grenada, Spain.

0148-0227/09/2008JD010073

equivalent radiance (NER) at 9.6 μm (channel 4) is on the order of 10^{-9} W cm^{-2} sr^{-1}, which is equivalent to the blackbody temperature of 88 K. Relying on the low noise level in the infrared range SABER is able to achieve a vertical resolution less than 2 km without degradation as altitude increases. These advantages place SABER in somewhat of a unique position with a high potential for studying the MLT region.

[4] SABER is a limb sounding 10-channel broadband infrared radiometer. Two bands, at 1.27 μm and 9.6 μm (O3_96 hereinafter) are used for ozone sounding. The focus of this validation research is on the O3_96 band for altitudes between 15 km and 70 km ($\sim$115–0.04 hPa). A companion paper to be submitted in the near future will address ozone validation using the 1.27-μm channel, which mainly focuses on the lower mesosphere to lower thermosphere daytime ozone.

[5] In section 2, SABER channel characteristics at 9.6 μm, the retrieval algorithms, error analysis, and version development are described. In section 3, validation approaches used in this study are discussed. SABER versus SBUV/2 (solar backscatter ultraviolet instruments) comparisons are discussed in detail in section 4. SBUV/2 provides data over the sunlit part of globe and its upper limit does not go above $\sim$52 km. In section 5, comparisons between SABER and the MIPAS (Michelson Interferometer for Passive Atmospheric Sounding) offline versions v4.61 and v4.62 data are performed. The two versions are substantially equivalent for ozone. The MIPAS data set broadens the validation possibilities from SBUV/2 because it extends the altitude range into the lower mesosphere ($\sim$70 km) and meanwhile provides day and night measurements. In section 6, MLS (Microwave Limb Sounder) v2.2 data are used to provide a further check on the SBUV/2 and MIPAS results. Section 7 includes discussion of SABER versus solar occultation measurements, and SABER versus ground-based measurements. SAGE (Stratospheric Aerosol and Gas Experiment) II is chosen among several well established solar occultation data sets, for example, HALOE (Halogen Occultation Experiment), SAGE III. Some related topics are discussed after the major comparison sections. Data artifacts are discussed using a probability approach in section 8. This approach is to inform SABER users about problematic regions and time frames of anomalous O_3 values. In section 9, time and space mismatch statistics are briefly examined. Section 10 provides a summary and conclusions.

2. SABER Measurements

2.1. SABER Orbital and Flight Information

[6] SABER/TIMED was launched into a 74.1° inclined, 625 km sun-synchronous circular orbit on 7 December 2001 [*Russell et al.*,1999; *Tansock et al.*, 2006]. SABER measures earth limb emissions in the infrared range from 1.27 μm to 17 μm, using a 10-channel broadband infrared radiometer to obtain radiances from several atmospheric species including CO_2 (15 μm and 4.3 μm), O_3 (1.27 μm and 9.6 μm), $O_2(^1\Delta)$ (1.27 μm), OH (2.1 μm and 1.6 μm), NO (5.3 μm), and H_2O (6.9 μm). These species play key roles in heating, cooling, photochemistry, and dynamics in the MLT region. Most targeted variables are retrieved successfully in SABER v1.07 data except for H_2O and CO_2. The fact that H_2O is in the strong line limit up to 80 km, combined with the nonlocal thermodynamic equilibrium (NLTE) effect, has posed profound challenges to its retrieval. Work is under way to further improve the temperature accuracy, which will significantly help the H_2O retrieval.

[7] SABER observations provide near-global coverage, and continuous measurements day and night. The SABER instrument observes the limb perpendicular to the TIMED spacecraft orbit plane. The spacecraft yaws every two months to ensure that the SABER entrance aperture is always pointing away from the sun [*Dakermanji et al.*, 1997]. As a result of the yaw SABER spatial coverage alternates approximately every 60 days from 83°S–52°N to 52°S–83°N. This yaw also prevents SABER from having symmetric daily local time coverage. Two local times for a given latitude, corresponding to the ascending and descending modes, are covered for each day and it takes about two months to approximately cover all local times.

[8] Once every 58 s, SABER scans up or down the Earth's horizon, collecting data over an altitude range from cold space (>400 km) down to the Earth's surface. The overall range of valid measurements is approximately from 12 km to 180 km. There are 96 scans in one orbit and approximately 1400 scans per day covering 14 bands spaced evenly in longitude. The corresponding along track sampling distance is $\sim$500 km.

2.2. O3_96 Channel Characteristics and Retrieval Algorithms

[9] SABER O3_96 channel characteristics and retrieval algorithms bear strong similarities to the O_3 channel used for LIMS (Nimbus 7 Limb Infrared Monitor of the Stratosphere) experiment of 1978/1979 [*Gille and Russell*, 1984; *Remsberg et al.*, 2007] but the SABER noise level is significantly lower owing to advancements in detector and electronics technology. Figure 1 shows the SABER O3_96 channel spectral range and filter function. The spectral interval covers the range of 925–1200 cm^{-1} ($\sim$9–11 μm), and the observed SABER end-to-end O3_96 spectral response function in range 1000–1150 cm^{-1} is near-flat above the 80% relative response points.

[10] Ozone has three vibrational normal modes, i.e., symmetric stretch, bending, and asymmetric stretch modes. The vibrational excited O_3 state is determined by all three modes. The frequency of vibration is 9.06 μm for the symmetric stretch mode, 14.2 μm for the bending mode, and 9.6 μm for the asymmetric stretch mode. The asymmetric stretch mode (9.6 μm) is by far the strongest band of all three. Among the relatively important gases in the infrared (H_2O, O_3, and CO_2), O_3 is the primary emitter in the 9- to 11-μm range with CO_2 at the 9.4-μm "hot band" being the only other significant emitter when conditions of nonlocal thermodynamic equilibrium (NLTE) exist, i.e., above $\sim$50 km altitude [*Mlynczak and Drayson*, 1990a, 1990b]. Local thermodynamic equilibrium (LTE) starts to fail when collision no longer dominates the population ratios between the higher and lower energy levels of the molecules. Under LTE conditions, the contribution from CO_2 is only a few percent to the total band integrated radiance. The SABER O3_96 retrieval algorithm includes both LTE and NLTE components. O3_96 retrieved from

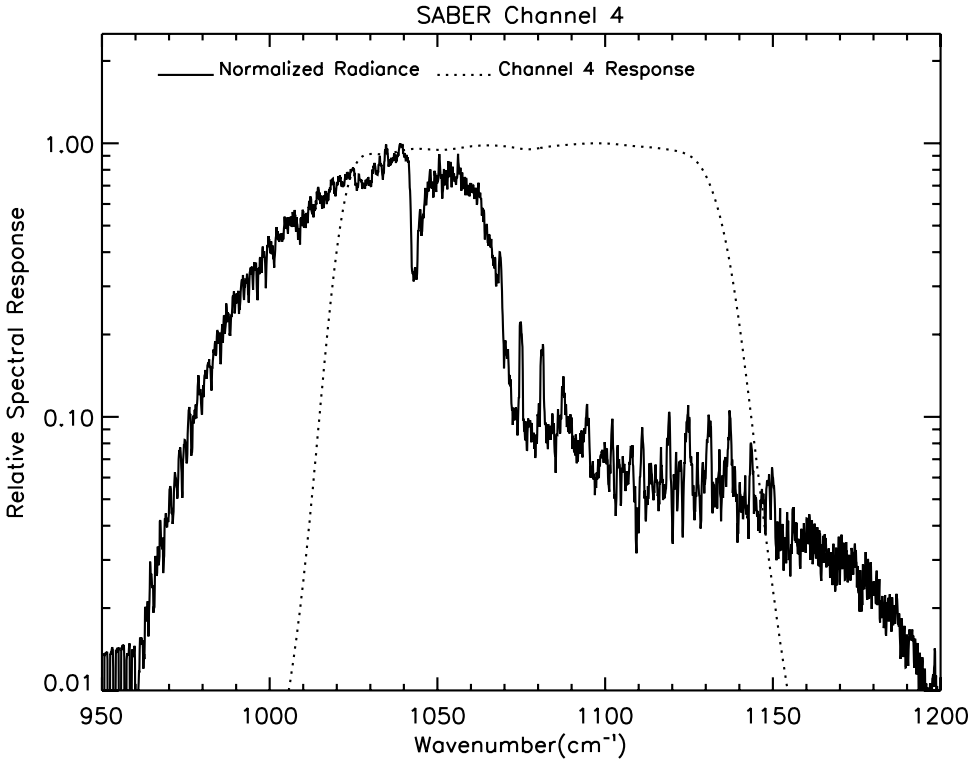

Figure 1. SABER channel−4 spectral range and the response filter function. The dark solid line is the normalized radiance, and the dotted line is the response filter function.

LTE and NLTE are merged over a 10-km altitude range (50−60 km) using a weighting kernel that varies linearly from 100% LTE at 50 km to 100% NLTE at 60 km.

[11] The forward model used in the SABER retrieval is the BANDPAK model described by *Marshall et al.* [1994]. For individual channels tables of emissivity growth versus pressure, mass path, and temperature were created for the forward model following the Emissivity Growth approximation (EGA) method described by *Gordley and Russell* [1981]. Under NLTE conditions, computing the table is a more challenging task due to the additional variables involved in the emissivity. Ideally line-by-line calculations that explicitly account for the departure from LTE in both the source functions and the transmittances are necessary, but instead, a fast algorithm developed by *Mlynczak et al.* [1994] combining NLTE and EGA was applied. In this approach only the different vibrational-rotational bands are treated separately. To compute the NLTE emissivity, an ozone T_v (vibrational temperature) model was developed as a part of the NLTE forward model. The ozone T_v model included 11 vibrational-rotational bands and a CO_2 "hot" band within the SABER filter range. This fast algorithm increases the computation speed by a factor of 10^4 yet maintains close agreement with the results of line-by-line calculations.

[12] In the inverse model an onion peeling algorithm [*Russell and Drayson*, 1972] is applied. The O_3 volume mixing ratio (vmr) in the limb tangent layer is adjusted for each iteration until the computed and measured radiances match to within the noise level (NER). This process begins at the highest altitude for which there is a sufficient signal-to-noise and proceeds down in altitude always holding the values retrieved at higher altitudes fixed at the vmrs retrieved at those altitudes. A constant O_3 vmr is assumed for the layers above the starting altitude to begin the retrieval. The effect of this assumption becomes negligible within about 5 km below the starting layer because of the limb geometry and the exponential increase of pressure with decreasing altitude. The SABER instrument includes a precise limb scan angle optical encoder that, along with the spacecraft ephemeris, provides excellent knowledge of the vertical spacing between radiance samples. Limb radiances are sampled every 0.4 km in altitude. In order to make maximum use of all radiance samples taken at ∼0.4 km increments, an interleave retrieval approach is used. For a given radiance profile, five retrievals are performed, each using retrieval points spaced five radiance samples apart; i.e., at 2-km increments. The next retrieval starts one radiance sample increment down in altitude from the first and the third one down from the second and so on. After the five retrievals are complete for a given limb scan event, the profiles are averaged to provide the resulting retrieved profile for that event. This approach makes maximum use of all radiance data and avoids the instability that results when retrievals are attempted at a vertical spacing that is less than the FOV (field of view) size (i.e., 2 km). The SABER vertical resolution is ∼2 km for all channels and all altitudes.

2.3. O3_96 Overview and Version Differences

[13] We first show the effect of the yaw and the corresponding local time coverage in Figure 2, and then provide an overview of global O3_96 and its temporal variation in Figures 3 and 4. The ascending and descending

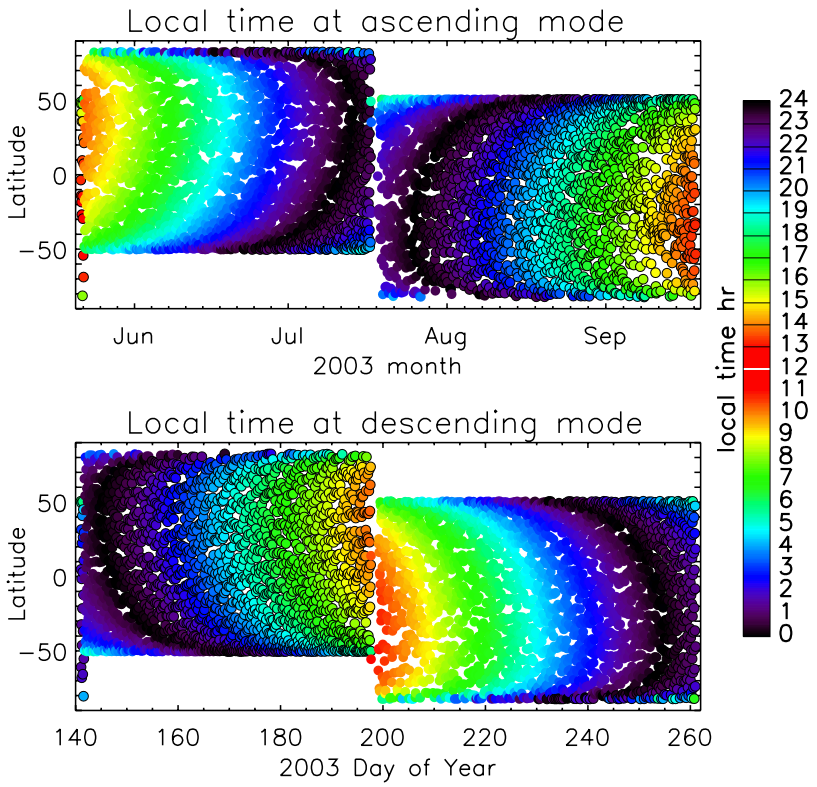

Figure 2. Latitude and local time coverage of individual SABER events (solid circles with color scaled by local time) during two consecutive SABER yaw cycles from 15 May to 15 September 2003. (top) Ascending mode measurements. (bottom) Descending mode measurements.

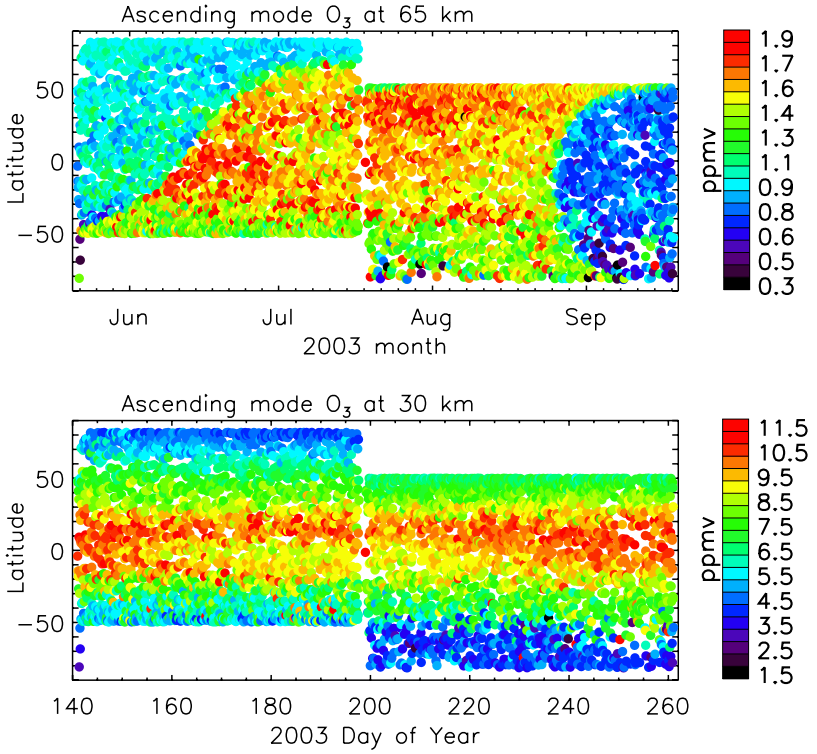

Figure 3. Ozone volume mixing ratios corresponding to the ascending mode in Figure 2. (bottom) At 30-km surface. (top) At 65-km surface.

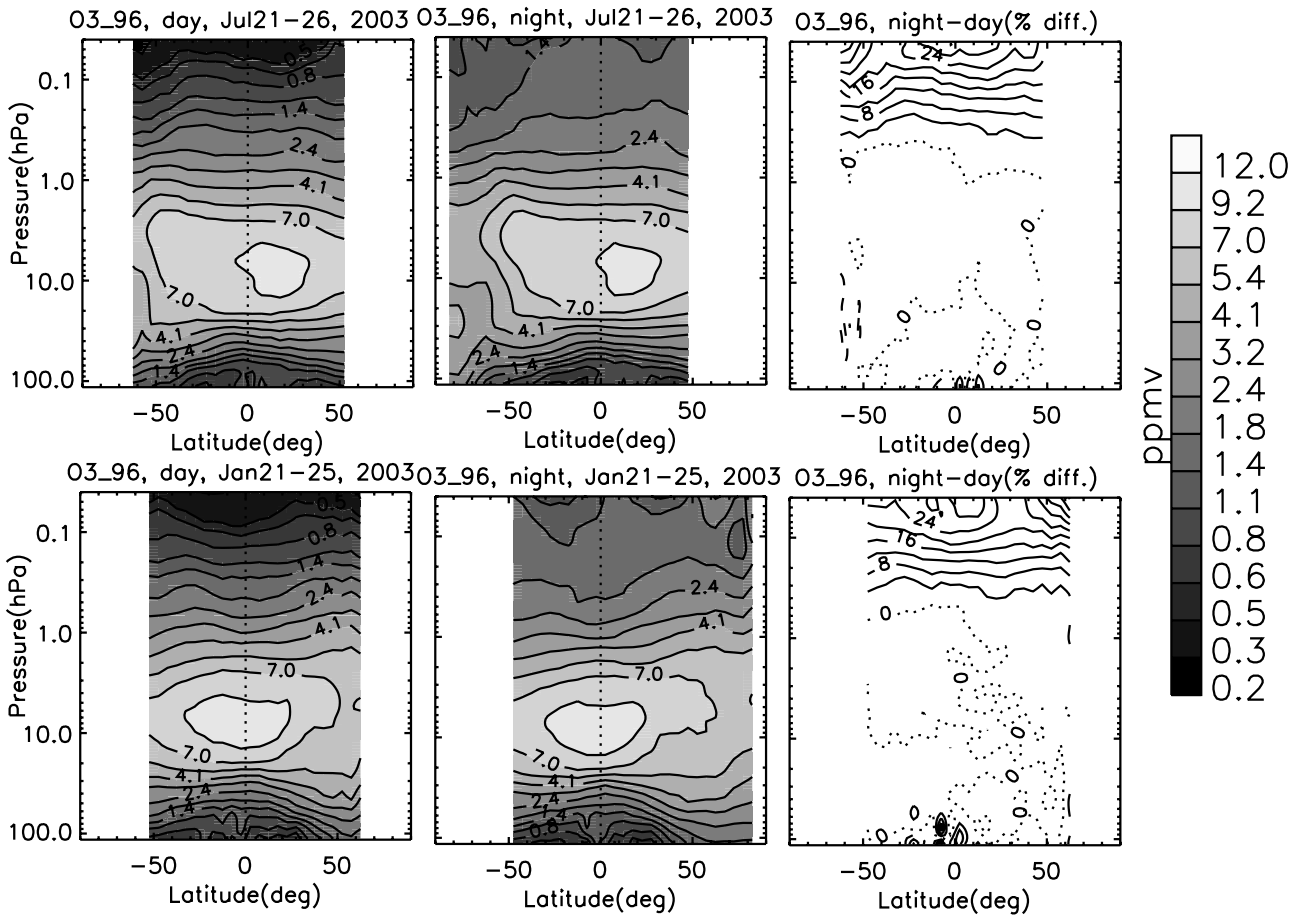

Figure 4. SABER v1.07 zonal mean O3_96 for day and night measurements, and the percent difference between the two, in (top) July and (bottom) January. Five consecutive days (with one missing day skipped) are chosen for each case.

modes roughly separate day and nighttime measurements except in polar winter or summer. For an ascending or descending mode only, all local times are roughly achieved within two consecutive yaw cycles (~4 months). When looking at an ascending or descending mode individually we can see that the local time change within 5 or 10 consecutive days is rather small. Figure 3 shows the O3_96 vmrs in the exact frame of Figure 2 (top) (ascending mode). Ozone at two altitudes, 30 km and 65 km, are shown to represent the distributions in the stratosphere and lower mesosphere, respectively. In Figure 3 (top) where the mesospheric O_3 is shown we observe contrasting high and low O_3 divided by the day and night (also see Figure 2, top). The transition zone is extremely narrow and the O_3 distribution overall resembles a ''plateau''-like structure. The low O_3 band extended into July is due to the existence of polar summer when sunlight remains all day clearly showing the diurnal effect on O_3 in the mesosphere. It appears that the lower mesosphere O_3 abundance does not show much variation with either space or longer timescales (i.e., >1 day). Figure 3 (bottom) shows drastically different characteristics, in which O_3 is strongly latitude dependent. The O_3 vmr is the largest at the equator and then decreases monotonically as latitude increases toward both hemispheres. Figure 4 shows the zonal mean O_3 latitude-pressure cross section in 2003 January and July for several consecutive days. It shows that at pressure levels >0.3 hPa the day-night difference is negligibly small. Nevertheless, the same type of plots for some other years indicate that the daytime stratospheric O_3 peak is slightly stronger than its nighttime counterpart (not shown). Dependence on latitude is the strongest around 8–10 hPa where the O_3 peak is located. Zonal means in January and July show similar structure but there is an asymmetry between the two. It is noted that in July the O_3 maximum at low latitudes occurs in a more northward location (~20°N) than in January. This asymmetry also exists in all other years of SABER O_3 data. This is likely dynamically driven and is probably related to hemispheric differences in the polar vortices and the strength of the ozone depletion.

[14] Figure 5 shows the differences between the O3_96 v1.06 and v1.07 releases. For accurate comparison we select pairs of profiles in the two versions with identical event indices that correspond to the same set of measurements. We chose all coincident pairs from four days including 21 March, 21 June, 21 September, and 21 December in 2003. Their mean percent difference and 1-σ standard deviation (gray shade) are computed. Day and nighttime measurements are performed separately. It can be seen that in both day and night, the v1.07 O3_96 is smaller in general

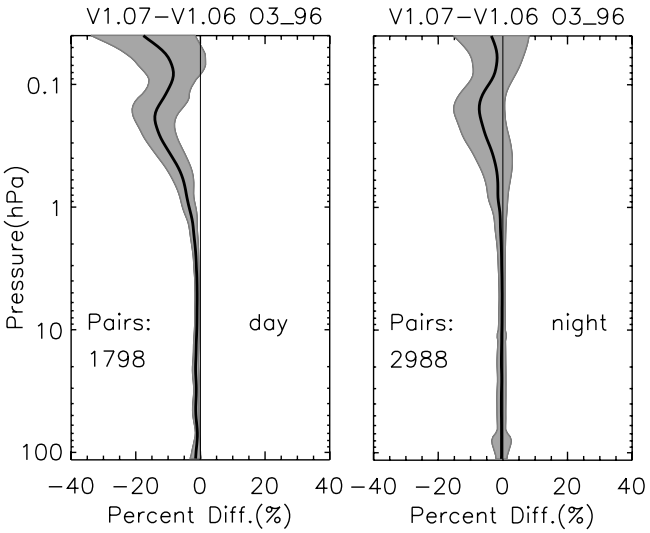

Figure 5. SABER v1.07 and v1.06 O3_96 difference. All events on 21 March, 21 June, 21 September, and 21 December 2003 are used. The pairs are searched by matching up the exact event indices. The solid line represents the mean percent difference, and the gray shade is 1-σ standard deviation. Day and nighttime measurements are performed separately.

but the daytime difference is much larger, reaching 15–20% in the mesosphere (<0.5 hPa), and with higher statistical significance. There is also a small difference (~2%) in the stratosphere in daytime. During nighttime on the other hand, the difference in the lower-altitude region (>1.0 hPa) is almost zero with extremely small scatter, while in the mesosphere the maximum difference is approximately 10%. The main difference between the two versions is in the mesosphere while in the stratosphere the difference is negligible.

2.4. Error Analyses

[15] Table 1 provides the itemized and total systematic and random errors under LTE conditions at six pressure levels covering the stratosphere. The O_3 error analysis was performed by taking an original "true" unperturbed O_3 profile, calculating the corresponding radiance profile using the forward model, and then perturbing the radiance profile by adding errors. Retrievals were then performed on the perturbed radiance profiles to obtain O_3. When the related error was estimated all remaining input parameters were set to their nominal values. The resulting error is defined as the 1-σ standard deviation of a large number of retrievals using the perturbed radiance profiles. The total error is the root sum square (RSS) of errors obtained for each error type. The onion peeling retrieval does not account for interlevel correlation since the limb viewing geometry heavily weights information in the tangent layer. Random error sources included detector noise and scan mirror "jitter." The O_3 responses to random error sources are reduced by a factor of $\sqrt{5}$ owing to the interleave retrieval approach. Ozone error induced by detector noise is extremely low, i.e., 0.5% maximum, compared to a much larger error of 8% due to "jitter," or pointing uncertainty due to the angular excursion of the instrument's line of sight within a sampling time period. Both detector and "jitter" induced random errors decrease rapidly with height. SABER detector error is ~20 times smaller than its LIMS counterpart computed using the V6 algorithm [*Remsberg et al.*, 2007]. The "jitter" height uncertainty in SABER is on the order of ~20 m. The "jitter" error was also halved from the error that existed in the LIMS O_3 measurement. The total precision in this altitude range varies from 8% to 1%, with the middle to upper stratosphere (<10 hPa) showing the best precision.

[16] Radiance bias errors due to calibration uncertainties are estimated to be about 1% on the basis of the laboratory calibration. SABER in-flight calibration (IFC) was done in the usual way by tying the IFC source in SABER to the ground calibration and using the IFC as a transfer standard. The radiance scale-factor is updated every other limb scan by using the IFC source and cold space to get the zero radiance response. The resulting systematic errors in retrieved O3_96 due to calibration errors vary from 2% to 5%. For each SABER channel end-to-end spectral responses were checked. The out-of-band response specification of $\sim 10^{-4}$ was met in all channels except at longer wavelength 14.9 μm. Spatial FOV (field of view) sidelobes due to off-axis scatter were checked by scanning the moon as the hot source against a cold background, and an off-axis rejection response of 10^{-5} or better can be achieved. The temporal response due to the electronics filter was carefully determined so that any amplitude or phase distortion can be deconvoluted properly. After the deconvolution, the overshoot, undershoot, and phase lag in the responses are removed almost perfectly. In general, the effects of instrument were characterized very well prior to the launch of SABER and they were deconvoluted accurately from the radiances in the Level1 product.

Table 1. Precision and Accuracy Estimates for SABER V1.07 Ozone Profiles[a]

	Pressure-Altitude					
Error Type	100 hPa	50 hPa	10 hPa	3 hPa	1 hPa	0.4 hPa
Random Errors						
Detector noise[b]	0.5	0.3	0.2	0.1	0.2	0.4
Jitter (20 m)	8	6	2	1	1	0.8
Total precision (RSS of noise and jitter, nearest %)	8	6	2	1	1	1
Systematic Errors						
Calibration (1%)	3	4	5	3	2	2
Line intensity (4%)	4	4	4	4	4	4
Line halfwidth (10%)	2	2	3	3	2	2
Band model[c]	8	5	3	2	1	0.5
T(P) error[d]	20	15	7	5	7	7
Total systematic error (RSS of terms, nearest %)	22	17	10	8	9	9
Expected Accuracy						
RSS of a and b, nearest %	23	18	10	8	9	9

[a]Some of the values given in this table are based on simulations using a standard atmosphere. Estimates are given as percentages.
[b]Detector noise and jitter errors are reduced by factor 1/2.236 owing to use of five interleaves.
[c]Band model errors are from comparisons to line-by-line for standard atmosphere.
[d]T(P) error is based on validation results discussed by *Remsberg et al.* [2008].

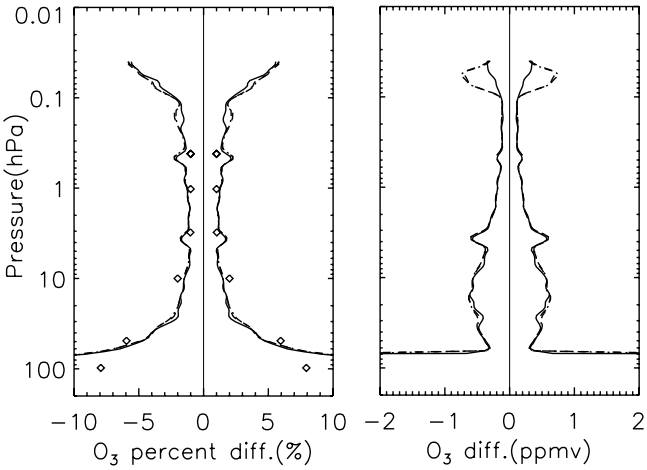

Figure 6. An empirical estimate of the precision based on repeatability test. The precision is given by the 1-σ standard deviation (STD) scatter of the up- and down-scan differences (black lines). The different line styles are for different sample numbers to ensure valid statistics. All coincidences in latitude range 10°S–10°N are used. The diamond signs are the SABER total precision scatter given in Table 1. (left) Precision by percent difference. (right) Precision by absolute difference.

[17] Uncertainties in spectral parameters will lead to inaccuracies in the band model results. Two error sources are considered, line intensity and pressure broadened line half-widths errors [*Smith and Gordley*, 1983]. Line intensities in HITRAN 2000 [*Rothman et al.*, 2003] are known to about 4%. Line half widths are known to about 10%. The error responses in O_3 in both cases indicate an error level (~2–4%) that varies only slightly with altitude. The monotonic error response to the line widths uncertainty was also shown in the LIMS O_3 analysis [*Remsberg et al.*, 2007]. Band model errors are obtained by comparing calculated radiances to line-by-line model results. These results show a bias of 0.5–8% that decreases rapidly as atmospheric pressure falls. It suggests that the LTE Band model performs the best in the middle to upper stratosphere. Kinetic temperature (T_k) induced systematic errors (7–20%) dominate the total systematic error throughout the entire altitude range, but especially in the lower stratosphere. The temperature error inputs are obtained from the *Remsberg et al.* [2008] validation paper. It is reported in this paper that SABER temperature shows a warm bias of 2–3 K in the lower stratosphere and a cold bias of 1–2 K from the upper stratosphere to the middle mesosphere. The estimate of SABER T_k bias error used in this analysis was taken from Table 1 of *Remsberg et al.* [2008]. These biases are critically dependent on errors in autonomous pressure registration (i.e., pressure retrieval) obtained using the "two-color" approach described by *Gille and Russell* [1984]. This approach uses both the narrow and wide CO_2 bands at 15 μm to retrieve temperature versus pressure independent of absolute pointing. The O3_96 retrieval is highly responsive to these temperature biases, and is showing rather large biases throughout the stratosphere. In summary, total systematic errors are much larger than total random errors at all altitudes, and are dominating the expected accuracy. The estimated accuracy varies between 9% and 23%, and is ~10% over the 10- to 0.4-hPa range.

[18] The estimated retrieved precision can be checked in orbit by calculating the standard deviation of a number of profiles that are measured under relatively stable atmospheric conditions, such as in the equatorial region or in the summer hemisphere where dynamical activity is reduced compared to the winter [e.g., *Russell et al.*, 1996; *Yokota et al.*, 2002]. The precision can also be estimated by using up- and down-scan pairs that should have high statistical repeatability since they are measured in very close local times (<10 min apart) and space coincidence thereby minimizing the impact of natural atmospheric variability. We chose pairs in a narrow equatorial latitude band (10°S–10°N). Figure 6 shows the standard deviation (STD) scatter of such pairs of profiles. Three overlapping time periods for days of year 180–183, 180–187, and 180–190, in 2003, are used to make reliable statistics. The estimated precision using absolute difference reaches a maximum of approximately 0.5 ppmv in the lower stratosphere at ~20 hPa, and decreases to 0.2–0.3 ppmv in the upper stratosphere. The percent difference is ~1–2% throughout the range from 50 to 0.4 hPa. The precision gets significantly worse at very low or very high altitudes. The scatter in the mesosphere (~0.04 hPa or ~70 km) did not exceed 5–6%, which is still excellent.

[19] The estimated total precision from retrieval tests (the diamond signs) and the repeatability deduced precision agree surprisingly well in nearly the whole range where the former is available. The measured repeatability at altitudes below 50 hPa is much larger than the retrieval estimates probably because the impact of clouds was not removed from the SABER database used for the estimate.

3. Methodology for Data Comparisons

3.1. Vertical Smoothing

[20] The comparisons are carried out by finding pairs of SABER and correlative data profiles that are coincident in both space and time. Statistics are computed on the same pressure levels for the two correlative data sets. Smoothing and interpolation must be applied prior to the comparisons. Smoothing procedure is applied to the data set with higher resolution to make its vertical resolution compatible with the other set. SABER is the data set being smoothed in most comparisons since its 2-km vertical resolution is higher than for most other large satellite data sets. A piecewise linear interpolation on log(pressure) is applied to both data sets so that they can be analyzed on common pressure grids. The common log(pressure) grids used in this paper are equivalent to ~0.4–0.5 km of geographic altitude.

[21] There are different approaches to perform the smoothing. *Froidevaux et al.* [2008] compared several smoothing approaches and concluded that their difference is small except in the range of large O_3 values or sharp gradients. We will use three different smoothing approaches based on different circumstances. Widely adopted Averaging Kernels (AKs) smoothing is applied to SABER O_3 in the SABER versus MIPAS comparisons because the MIPAS vertical resolution varies considerably in its whole vertical range. Other smoothing approaches may not be as precise as

the AKs. For each single SABER O_3 profile the formula $x_{smooth} = \hat{x}_a + A \cdot (x_h - x_a)$ is applied, where x_h is the high-resolution SABER profile that is linearly interpolated to the 0- to 120-km altitude grids, A is the Averaging Kernel matrix, x_a is the a priori O_3 profile for the MIPAS offline O_3 product, and $\hat{x}_a$ is the MIPAS retrieved profile when the true state of the atmosphere is equal to the a priori x_a. The disadvantage of the AK method is that the outcome will be severely affected by any singularities in the domain. This can be taken care of by removing the singular O_3 values in the domain when the sum is calculated.

[22] We use a fast Fourier transform (FFT) low-pass smoothing approach to smooth SABER profiles for comparisons with SBUV/2 and AURA/MLS ozone profiles. In the SBUV algorithm [*Bhartia et al.*, 1996], a series of defined pressure levels are halved from the previous ones so that in log(pressure) coordinates it is reasonable to use FFT smoothing because the resulting point spacing is equal. AURA/MLS also shows nearly unchanged vertical resolution between 200 hPa and 0.04 hPa. The FFT smoothing can function very well under the condition that the upper and lower boundary issue is well taken care of.

[23] In the SABER versus SAGE II, ozonesonde, and lidar comparisons SABER averaging kernels (a Gaussian form with half-maximum full width to be 2 km) are applied to these correlative data sets because these measurements have comparable or higher vertical resolution than SABER.

3.2. Coincidence Criteria

[24] The closest coincident pairs of O_3 profiles were found by using the criteria of 10 degrees in longitude, 2.0 degrees in latitude, and 2.0 h in time. The stronger restriction in latitude than in longitude is adopted owing to the quasi zonal symmetry of the large-scale flow in the middle to upper atmosphere. Within the constrained box the pair with the minimum geographic distance is chosen as the closest coincidence.

[25] Ozone abundance can have significant day and night difference above 50 km and therefore day and night comparisons are conducted separately. Model calculations [e.g., *Ricaud et al.*, 1996] do not show rapid O_3 vmr changes over a 2-h period except near twilight. There is however no uniform standard for choosing this criterion; that is, many other validation studies choose different criterion boxes [e.g., *Cortesi et al.*, 2007]. The given time interval can be considered large if the O_3 varies in a shorter timescale, such as around sunrise or sunset. In such cases the O_3 vmrs in one pair could present drastic day and night differences. We will examine such occurrences in a later section (section 8). In parallel to this, strong agreement does not necessarily mean that the coincidence criteria are perfectly valid. Rather, it could be due to an undisturbed atmospheric condition. Aside from the day and night consideration we also separate different latitude zones and seasons to roughly separate the different ensembles.

3.3. Statistics of the Coincidence Pair Differences

[26] The goal of the validation study is to quantify the systematic and random differences of the SABER O_3 from the true state of the atmosphere. Because the true state of the atmosphere is never known, in practice we compare the current data set to other well established data sets. The difference between a pair of coincident profiles is attributed to a series of factors, such as the systematic and random errors from the individual data sets, the errors caused by spatial and temporal mismatch, and the errors caused by different vertical resolution. Ideally these errors should be assessed individually [e.g., *von Clarmann*, 2006]. The error caused by incompatible vertical resolutions is reduced significantly by the vertical smoothing procedure, and the mismatch error will be discussed later in this paper. The mismatch induced error bias is in fact negligibly small in most cases with some exceptions. In high-latitude comparisons for example, the mismatch can increase the bias by $\sim 1-2\%$. The statistical moments of the O_3 differences between SABER and correlative data sets will be evaluated on the basis of the combined errors of the individual data sets.

[27] For a given pressure level j we compute the mean percent difference of all the coincident pairs (N total) as $\bar{\Delta}_j = \frac{1}{N}\sum_{i=1}^{N}\Delta_{j,i} = \frac{1}{N}\sum_{i=1}^{N}\frac{2(x_{j,i}-y_{j,i})}{(x_{j,i}+y_{j,i})}$, with x and y representing SABER and the correlative data measurements, respectively. The 1-σ standard deviation is defined as $\sigma_j = \sqrt{\frac{1}{N-1}\sum_{i=1}^{N}\left(\Delta_{j,i} - \bar{\Delta}_j\right)^2}$. The precision of the mean percent difference is defined by the standard error of the mean (SEM), as $p_{\bar{\Delta}_j} = \sigma_j/\sqrt{N}$. It is called bias when the mean difference exceeds the SEM and is proven consistent in all comparisons. The bias is zero within the total uncertainty of $\sigma_{\bar{\Delta}_j} = \sqrt{p^2_{\bar{\Delta}_j} + error^2_{SABER,sys} + error^2_{corr,sys}}$, where $error_{SABER,sys}$ and $error_{corr,sys}$ are systematic errors of SABER and the correlative data set, respectively. If the measurements from both data sets are valid the standard deviation σ_j is expected to be comparable to the combined random error of the two data sets, as $\sqrt{error^2_{SABER,rnd} + error^2_{corr,rnd}}$. When combined random errors are computed, the errors resulting from the higher-resolution data set should be reduced accordingly owing to the application of the smoothing procedure. In regions of strong atmospheric variability such as in the polar winter region, the standard deviation is often larger than the combined random error, depending on how the random errors of the individual data sets are computed.

3.4. Detection of Unusual Profiles

[28] Retrieved SABER O3_96 occasionally shows an anomalous vertical distribution or unrealistically large values in some lower stratosphere regions, and a proper screening process is needed to remove some extreme values from the statistical set. Some of these occurrences are probably associated with excessive attenuation by PSCs (polar stratospheric clouds) along the tangent path which leads to unaccounted for emission in the ozone channel and therefore biased retrievals [*Remsberg et al.*, 2007]. This interference will be accounted for and properly screened in a future version of SABER O3_96.

[29] One approach to find such profiles is by examining whether the probability of the differences between the coincident pairs follows a Gaussian distribution. It is argued to be the Gaussian if both data sets behave "normally." In other words, unusual behavior of either data set will lead to deviation from the Gaussian.

[30] To conduct the test, we first normalize the series as $\Delta_{j,new} = \frac{\Delta_j - \bar{\Delta}_j}{\sigma_j}$, and then start to build the coincidence

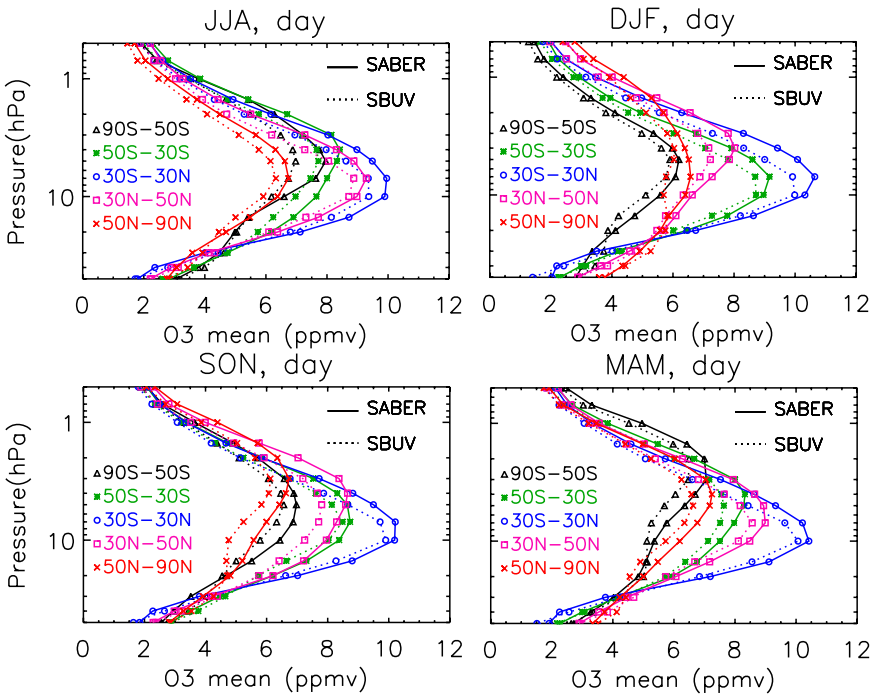

Figure 7. Mean O_3 volume mixing ratio profiles of the daytime comparisons between SABER and SBUV/2. The different seasons, JJA (June, July, and August), DJF (December, January, and February), SON (September, October, and November), and MAM (March, April, and May), and the five latitude bands (see text) are analyzed separately. All coincidences in 2002 and 2003 are included.

frequency by setting the bin width as 0.5. The number of bins is determined by the minimum to maximum values of the $\Delta_{j,new}$. The curve of the coincidence frequency is then obtained by counting the $\Delta_{j,new}$ values in each bin. A Gaussian with expectation of $\bar{\Delta}_j$ and variance of σ_j^2 is taken as a guide profile.

[31] The area defect and gain of the above built frequency curve from the corresponding Gaussian provides a "warning sign" of unusual behavior. In regions and time frames where the deviation is large caution should be used when selecting profiles. This deviation mostly results from erratic shapes or values in a minority of profiles in either of the data sets. This will be clearly shown in a latter section. On the other hand, the probability distribution could be perfectly Gaussian but still the profiles show anomalous features. This is because a majority of the profiles have consistent "unusual" or "nonphysical" behavior.

4. Comparisons With SBUV/2 Data

4.1. SBUV/2 Measurements

[32] The second-generation solar backscatter ultraviolet instruments (SBUV/2s) on NOAA 9, 11, 14, 16, and 17, are nadir-viewing instruments that are used to infer total ozone and ozone vertical profiles by measuring sunlight scattered from the atmosphere in the ultraviolet spectrum. SBUV/2 data are considered among the most reliable historical ozone profile records to date [e.g., *Wild et al.*, 2005; *Nazaryan et al.*, 2007]. The data we used came from the SBUV Version 8 data DVD. The DVD includes ozone data measured by the NOAA 16 satellite in the time period 2000–2003. NOAA 16 was launched in September of 2000 and remains operational to date. It is in a sun-synchronous local afternoon crossing time of 1420 local time (LT) in the ascending node. The IFOV (instantaneous field of view) is 180 km × 180 km. A complete wavelength scan is taken every 32 s to produce one retrieved profile. In the V8 algorithm 12 wavelengths from 256 nm to 340 nm are selectively used depending on the solar zenith angle of the observations in order to maintain its sensitivity to ozone changes in the lower atmosphere. The DVD includes all the retrieved profiles that have properly converged.

[33] In the DVD the SBUV ozone profiles were given on 15 pressure levels from 50 hPa to 0.5 hPa, corresponding to ~20 km to 55 km in geographic altitude. The vertical resolution of SBUV/2 O_3 data is constrained by the total ozone measurements, and is ~6 km in the 50 to 0.5-hPa range. SBUV/2 errors are the largest in the lower stratosphere, for example, ~12% at 50 hPa, decreasing to ~5–6% throughout the stratosphere, and increasing rapidly above 0.5 hPa [*Bhartia et al.*, 1996]. According to the previously described procedure a low-pass FFT smoothing is applied to all the SABER O3_96 profiles individually before the comparisons are performed.

4.2. Comparison Results

[34] Figure 7 shows the O_3 vmr mean profiles for both SABER and SBUV/2 based on the coincident pairs of profiles from each data set. Different latitude bands (90°S–50°S, 50°S–30°S, 30°S–30°N, 30°N–50°N, and 50°N–90°N) and different seasons are analyzed separately. The seasonal grouping is December, January, February (DJF); March, April, and May (MAM); June, July, and

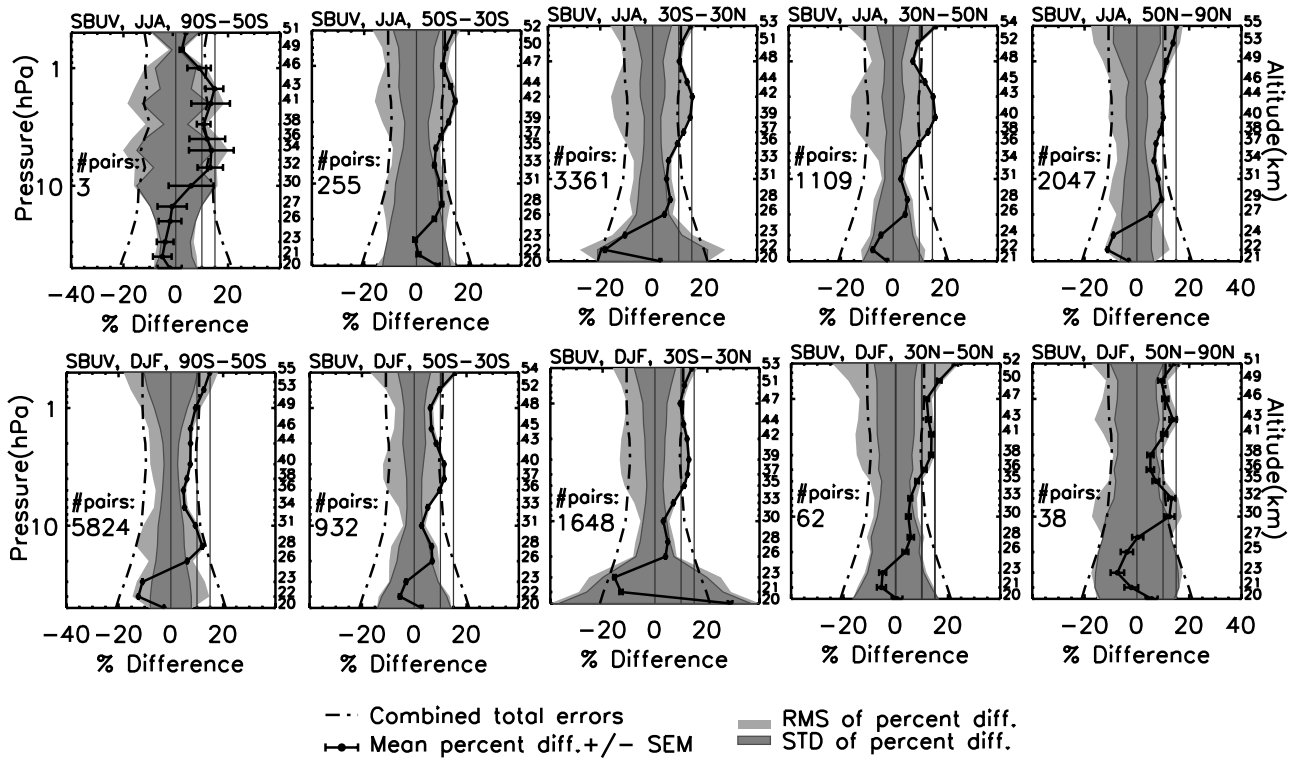

Figure 8. Ozone percent difference statistics and the combined total errors for SABER and SBUV/2 comparisons. Numbers of coincidences are indicated. The coincident box is 2.0 h in time, 2.0 degrees in latitude, and 10 degrees in longitude. Altitudes for each panel are indicated on the right-hand *y* axes. (top) JJA season. (bottom) DJF season. Guide lines of 10% and 15% are plotted.

August (JJA), and September, October, and November (SON).

[35] In all panels of Figure 7 the two data sets agree reasonably well but an offset of 1–1.5 ppmv is clearly seen. In all comparisons SABER O_3 is larger than SBUV/2 O_3 in the middle to upper stratosphere (20–0.5 hPa) but is lower in the lower stratosphere. The absolute difference is the largest in the equatorial and middle latitudes, and is the smallest in the summer high latitudes. We also note that O_3 mean profiles in JJA and DJF show strong interhemispheric symmetry in both O_3 distribution and magnitude. Fall and spring (MAM and SON) also show such symmetry. Generally, in the fall and spring the O_3 absolute differences are comparable to or slightly larger than the winter and summer cases.

[36] Mean percent differences of O_3 between SABER and SBUV/2 and the corresponding errors are shown in Figures 8 and 9. The signs of the biases are determined by SABER O_3 minus the correlative data O_3 (SBUV/2 here), as is also true for all other comparisons performed in this paper. The combined errors were obtained by computing the root sum square (RSS) of SABER total error (Table 1) and SBUV/2 total error [*Bhartia et al.*, 1996]. Both measurement and model uncertainties were included in the SBUV/2 errors. SABER random errors are reduced by a factor of $\sqrt{3}$ owing to the FFT smoothing.

[37] It is clearly seen that in all panels of Figure 7 the negative and positive mean differences are divided around 20–25 hPa (~27–23 km). The negative biases vary from 10% to 20% but in most cases they are lower than 15%. In nearly all cases the negative biases stay within the combined total error reasonably well except in the SON 90°S–50°S comparisons where they exceed the combined total error by a few percent. Positive biases exist in a large portion of the middle to upper stratosphere (~20–0.5 hPa), varying from 5% to 17%. In JJA in the equatorial region and middle latitudes, the biases are consistently large in the range 35–45 km, exceeding the combined total error by ~5–6%. The summer hemisphere is slightly worse. In DJF, the biases overall have a similar distribution in altitude or latitude but the magnitude is smaller. In both seasons agreement in summer high latitudes is the best, staying within ~10%. The fall and spring comparisons also highlight the 35- to 45-km range as showing the largest positive biases, and for both fall and spring the largest bias is in the 30°N–50°N range.

[38] The 1-σ standard deviation is larger in the winter hemisphere and decreases toward the summer hemisphere. Unlike biases, the standard deviation seems to be strongly correlated to the level of atmospheric disturbances. It is noted that the RMS (root mean square of the percent differences) and the biases are in close agreement, which indicates that the errors are dominated by the systematic errors. Regarding the larger positive biases between 35 km and 45 km it is interesting to note that this vertical range is right above the O_3 peak where the O_3 rapidly decreases, showing the strongest gradient. A small difference in slope can lead to rather large absolute differences. It is noted from Figure 7 that the SBUV/2 O_3 slope is consistently smaller than the SABER O_3 slope above the O_3 peak, with the two

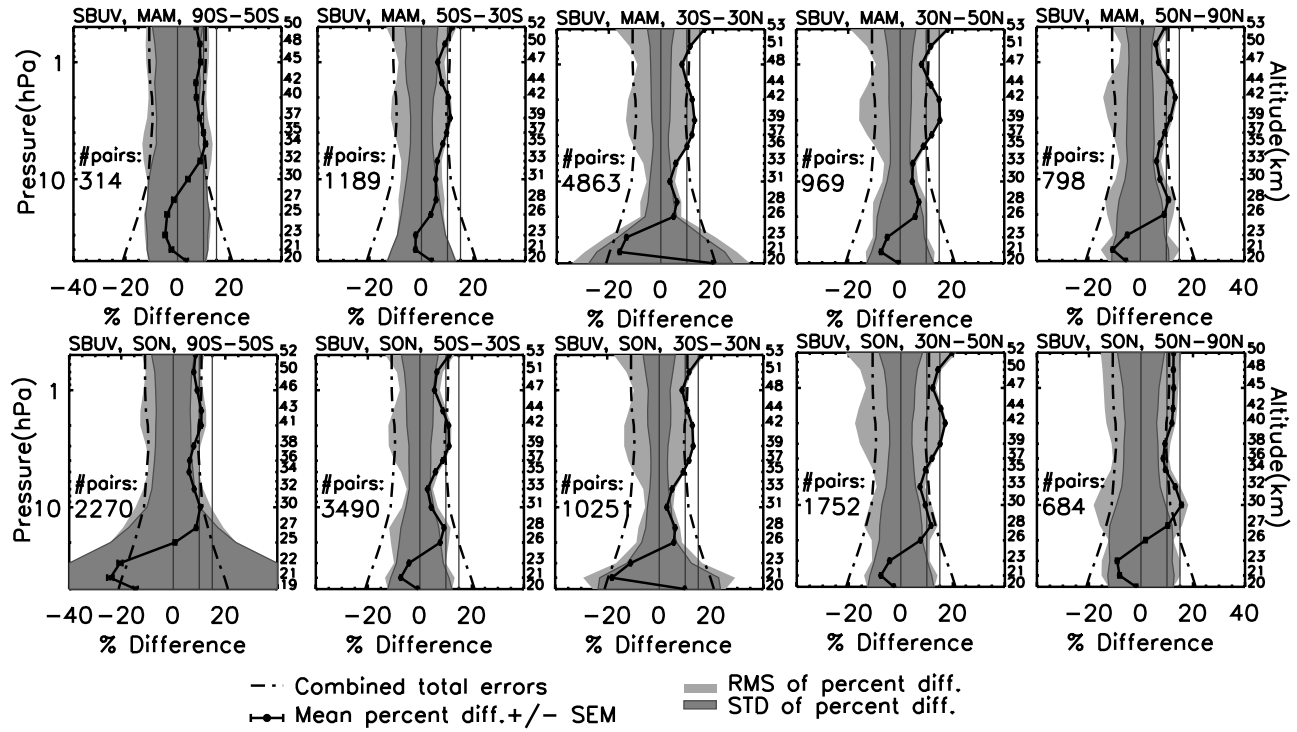

Figure 9. Same as Figure 8 except for SON and MAM seasons.

being closer at the upper altitudes around 0.5–1 hPa but they then separate gradually as the altitude decreases. One reason for the lower biases in the polar summer is the smaller slope attributed to the smaller O_3 peak. The polar winter comparisons, on the other hand, are inconclusive because of the fewer daytime measurements near the polar night region. The few available coincidences in this region indicate smaller percent differences than those in the middle latitudes.

5. Comparisons With ENVISAT/MIPAS Data

5.1. MIPAS Measurements

[39] The MIPAS instrument is a Fourier transform infrared spectrometer operating onboard the environmental satellite ENVISAT launched by ESA on 1 March 2002 [*Raspollini et al.*, 2006]. MIPAS ceased operation in March of 2004 but resumed activity again in January 2005 with lower spectral resolution. The instrument takes measurements globally both day and night by limb viewing in the middle infrared spectral range from 685 cm^{-1} (14.6 μm) to 2410 cm^{-1} (4.15 μm). MIPAS is a high spectral resolution instrument which can resolve the majority of individual atmospheric spectral lines at high altitudes (i.e., >52 km). In the offline analysis performed by ESA (European Space Agency), a set of narrow spectral intervals are carefully chosen so that the retrieval is less affected by the uncertain spectral data, interference from other species, and the NLTE effect. The orbital track of ENVISAT/MIPAS is near-circular, with an inclination angle of 98°. A limb sequence (or scan) is composed of 17 spectra that are measured at different tangential altitudes from 6 to 68 km acquired in 76.5 s. During each orbit MIPAS performs 75 limb scan sequences plus measurements for instrument calibration.

[40] The operational analysis of MIPAS Level2 O_3 data are used in this study. Data are processed offline by ESA with no requirement of near-real time (within 3 h of measurements) operation. Reanalysis of the measurements improved the geolocation registration and the Optimized Retrieval Model allowed an extended height range up to 73 km. A highly detailed validation of MIPAS O_3 has been conducted by *Cortesi et al.* [2007].

[41] The MIPAS vertical resolution is approximately 3 km below 42 km, 5 km between 42 km and 50 km, and 8 km above 50 km. MIPAS offline averaging kernels and the corresponding mean O_3 profile are provided at http://www.ifac.cnr.it/retrieval/auxiliary.html for download. The AK smoothing is applied to every SABER O3_96 profile before the comparisons were performed.

5.2. Comparison Results

[42] The same analyses were performed for SABER and MIPAS as was done with the SBUV/2. In addition, MIPAS enables us to conduct nighttime and lower mesospheric comparisons. The comparisons were conducted using all the coincidences from July 2002 to March 2004.

[43] Figure 10 shows the mean O_3 profiles for SABER versus MIPAS comparisons in day and night, and in JJA and DJF. We note the excellent agreement between the two data sets, i.e., showing far better agreement in daytime in all latitude bands than in the SBUV/2 related comparisons. Although indisputably SABER is still biased high in the middle to upper stratosphere, the absolute difference rarely exceeds 0.6 ppmv. The slopes of the two data sets are very close to each other in all cases. We also can see that both data sets captured the day and night difference in the lower mesosphere (50–70 km). The mean profiles show very good agreement in the lower mesosphere. In the lower

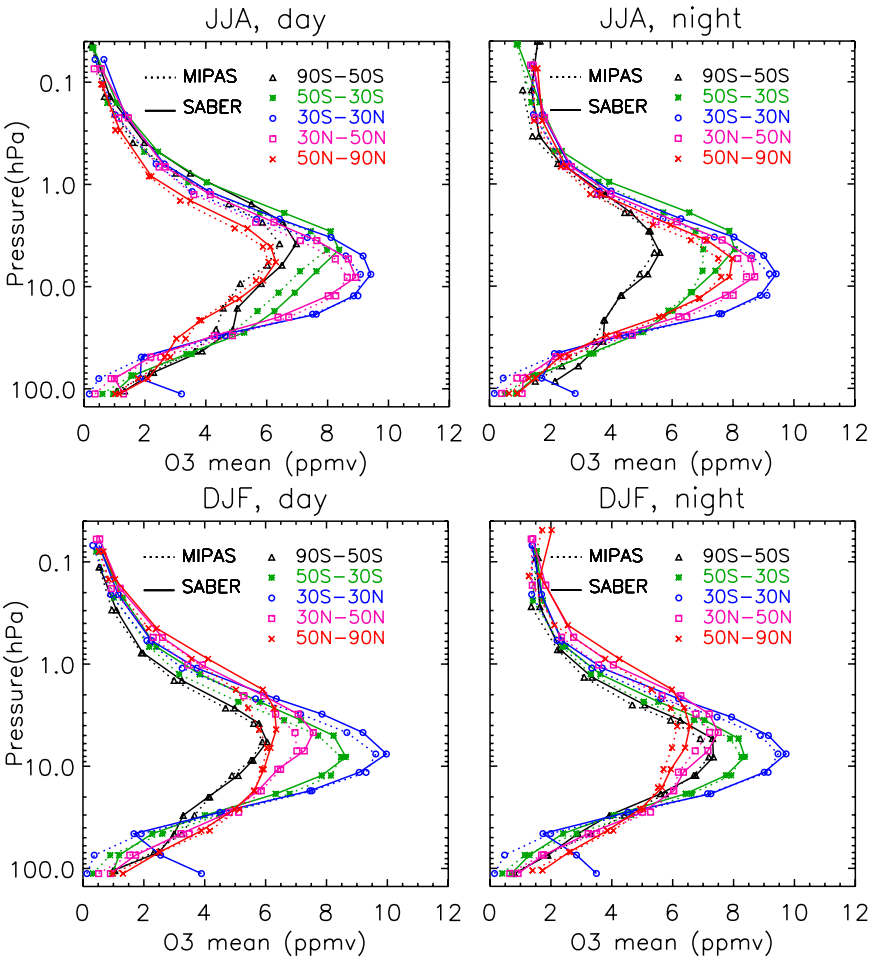

Figure 10. Mean O_3 volume mixing ratio profiles of the day and nighttime comparisons between SABER and MIPAS offline product for (top) JJA and (bottom) DJF seasons and (left) day and (right) night. All coincidences from July 2002 to March 2004 are included.

stratosphere (>50 hPa) SABER O_3 shows unrealistically large values in the equatorial region. This is a feature that appears in all cases, which is most likely caused by the unfiltered cloud effect.

[44] Figures 11 and 12 show the mean percent differences, 1-σ standard deviations, and combined errors in JJA and DJF for day and night. The systematic and random errors were adopted from the Oxford University MIPAS website at http://www.atm.ox.ac.uk/group/mipas/err. In the MIPAS error analysis, six groups of error profiles, based on six types of atmospheres are provided, i.e., middle latitude daytime, middle latitude nighttime, polar winter nighttime, equatorial daytime and composite. All six groups of errors are used in our comparisons. Note that since we do not provide SABER error table in the NLTE region above 0.4 hPa (~55 km), we use the values at 0.4 hPa throughout the range 55–70 km to prevent an abrupt jump in the combined errors. In such conditions the real combined errors could be larger than what is shown here.

[45] In the daytime comparisons below 50 km in most cases the mean percent differences are <10–12%, staying within the range of combined systematic errors except for 50°S–30°S in the DJF comparisons. In this latter case the positive bias is exceptionally large and exceeds the combined systematic error by ~5–7% in range ~40–50 km (~3–0.8 hPa). On average, the upper stratospheric bias in equatorial and middle latitude (50°S–50°N) daytime comparisons only exceeds the combined error by ~2–3%. In the daytime mesosphere (50–70 km) the mean percent differences are large in regions other than the polar latitudes. In the latitude range 30°S–50°N, the bias increases rapidly above 50 km. The better agreement in the polar latitudes again suggests that strong disturbances (i.e., large standard deviation in polar winter) are not related to the large biases.

[46] The nighttime comparisons show overall better agreement throughout the entire altitude range and in all latitudes. The stratospheric biases are <10% and are within the combined systematic error in nearly all cases with one exception in JJA winter middle latitudes. The agreement in the lower mesosphere (50–70 km) is also notably better (~20% or lower) than daytime partly owing to the fact that nighttime O_3 is higher than in daytime in this range. Since O_3 values are very low in the lower mesosphere, percentage differences will be large, in which case absolute difference could instead be a better index for comparison.

[47] The standard deviations and the combined random errors agree well in nearly all latitude bands with rare exceptions, and this is mostly attributed to the carefully

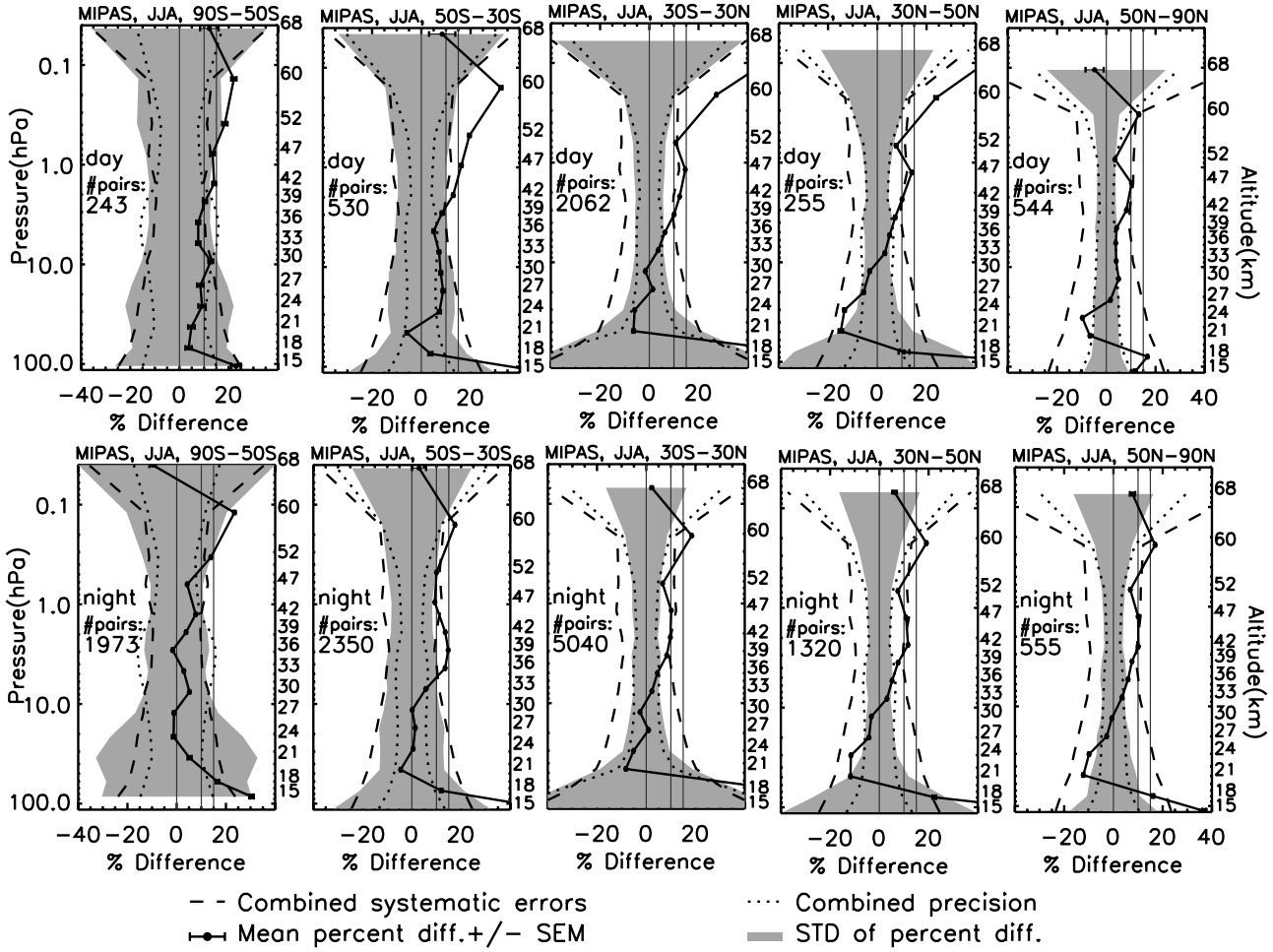

Figure 11. Ozone percent difference statistics and the combined errors for SABER and MIPAS comparisons in JJA season. Systematic and random errors are plotted separately because they were provided individually. Altitudes for each panel are indicated on the right-hand *y* axes. (top) Daytime comparisons. (bottom) Nighttime comparisons. Guide lines of 10% and 15% are plotted.

considered multitype atmosphere in the MIPAS random error computational regimes. It is likely that atmospheric variability was included in their random error computations.

6. Comparisons With AURA/MLS Data

6.1. MLS Measurements

[48] MLS (EOS microwave limb sounder) is onboard the AURA satellite launched on 15 July 2004, to provide information on Earth's troposphere, stratosphere, and mesosphere. MLS measures millimeter and submillimeter emission by scanning the earth atmospheric limb every 24.7 s (more than twice as fast as SABER) in the AURA velocity vector direction. AURA is in a sun-synchronous near-polar orbit (98° inclination) with a 1345 LT ascending equatorial crossing time. The day and night are therefore equally covered each 24-h period. MLS provides 240 scans per orbit or 3500 scans per day, giving along-track and cross-track resolution approximately of 200 km and 6 km, respectively. Unlike SABER, the MLS orbital plane has a larger inclination angle and the scans are within the orbital plane, which results in equal numbers of scans up to 82° north and south.

[49] MLS measurements are made in five spectral bands, at 118 GHz (2.54 mm), 190 GHz (1.58 mm), 240 GHz (1.25 mm), 640 GHz (0.47 mm), and 2.5 THz (0.119 mm) [*Waters et al.*, 2006]. The most recent v2.2 level2 O_3 standard product at 240 GHz is used in this study. The O_3 v2.2 and v1.5 products have been validated by *Froidevaux et al.* [2008].

[50] The scientifically useful range of MLS v2.2 O_3 is 215−0.02 hPa (∼11−75 km). Ozone average values in v2.2 are approximately 10% larger than in v1.5 in the upper stratosphere (http://mls.jpl.nasa.gov/data/datadocs.php), which potentially makes the higher-version data agree better with SABER O3_96.

[51] The vertical resolution of MLS is roughly 3 km between 250 hPa and 0.1 hPa (∼65 km), and degrades to 5 km at 0.05 hPa (∼70 km). Using pressure coordinates the log(pressure) points remain equally spaced throughout the 100- to 0.04-hPa range. Similar to what we have done for SABER versus SBUV/2 comparisons, a FFT smoothing is applied to each SABER profile to better match the MLS vertical resolution. Three years of data from 2005 to 2007 are used in the comparisons. Three screening indices, status field (= 0), quality (>0.4), and convergence (<1.8), are used

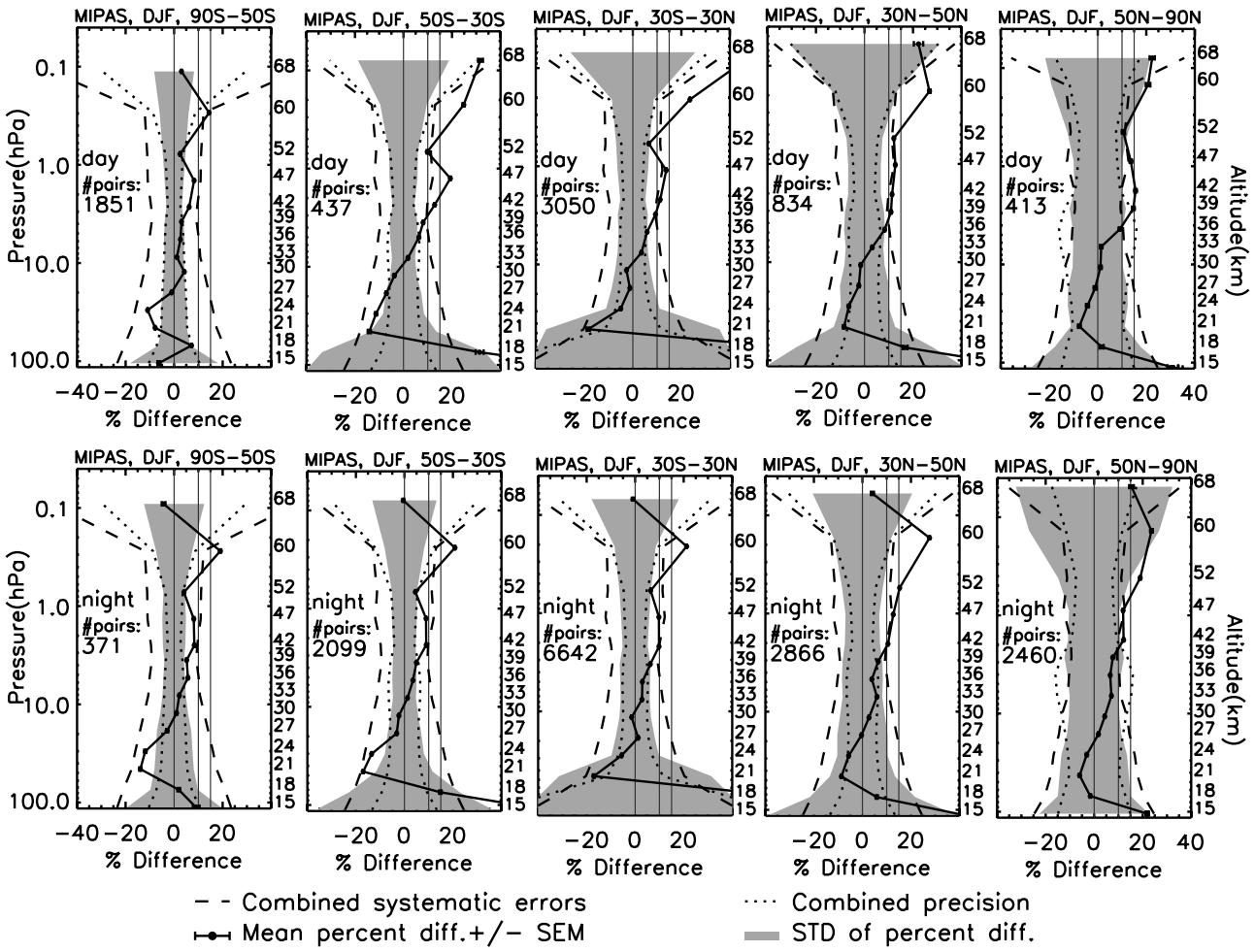

Figure 12. Same as Figure 11 except for DJF season.

to remove some unqualified MLS profiles prior to the comparisons.

6.2. Comparison Results

[52] Figure 13 shows the mean O_3 profiles for SABER and MLS in JJA and DJF, and for day and night. There is overall good agreement for both day and night and for different latitude bands, but the aforementioned stratospheric (20–2 hPa) high bias in SABER is larger (>0.9 ppmv) than in the MIPAS results. We also note that in the lower stratosphere (>50 hPa) the SABER mean O_3 clearly reflects the large values in equatorial region in all panels, which agrees with the MIPAS results. In the southern polar winter lower stratosphere SABER O_3 shows significantly larger values than in the MIPAS comparisons. This is probably because a larger fraction of profiles with anomalous stratospheric values fell into coincidences in SABER and MLS comparisons. This is likely circumstantial instead of being caused by any failed screening procedure. In a later section we will discuss these anomalous profiles and their occurrence.

[53] Ozone percent difference analysis is shown in Figures 14 and 15. For MLS we used the RMS of the single profile precision as the random error estimate, and the 2-σ systematic uncertainty as the systematic error. In the stratosphere at ~35–45 km the daytime bias is the largest in the equatorial region and middle latitudes, which agrees with the SBUV/2 results. The bias is however smaller than in the SBUV/2 comparisons, barely exceeding ~15%. In other cases of the stratospheric comparisons the biases are within or slightly above ~10%. The nighttime comparisons in the stratosphere show slightly better agreement than the daytime comparisons by ~1–2%. In the mesosphere (50–70 km) the mean percent differences remain around 20–25% up to ~60 km and then rapidly increase to >40%. Unlike MIPAS, the MLS day and night comparisons in the mesosphere show only a small degree of difference, with the nighttime percent difference being somewhat smaller above 60 km. The upward degradation of MLS precision starts from rather low altitudes; that is, it gets worse rapidly above 40 km (~2–3 hPa). The standard deviations also reflect this vertical distribution.

7. Comparisons With Solar Occultation and Ground-Based Measurements

[54] In this section comparisons were performed with satellite solar occultation and ground-based measurements.

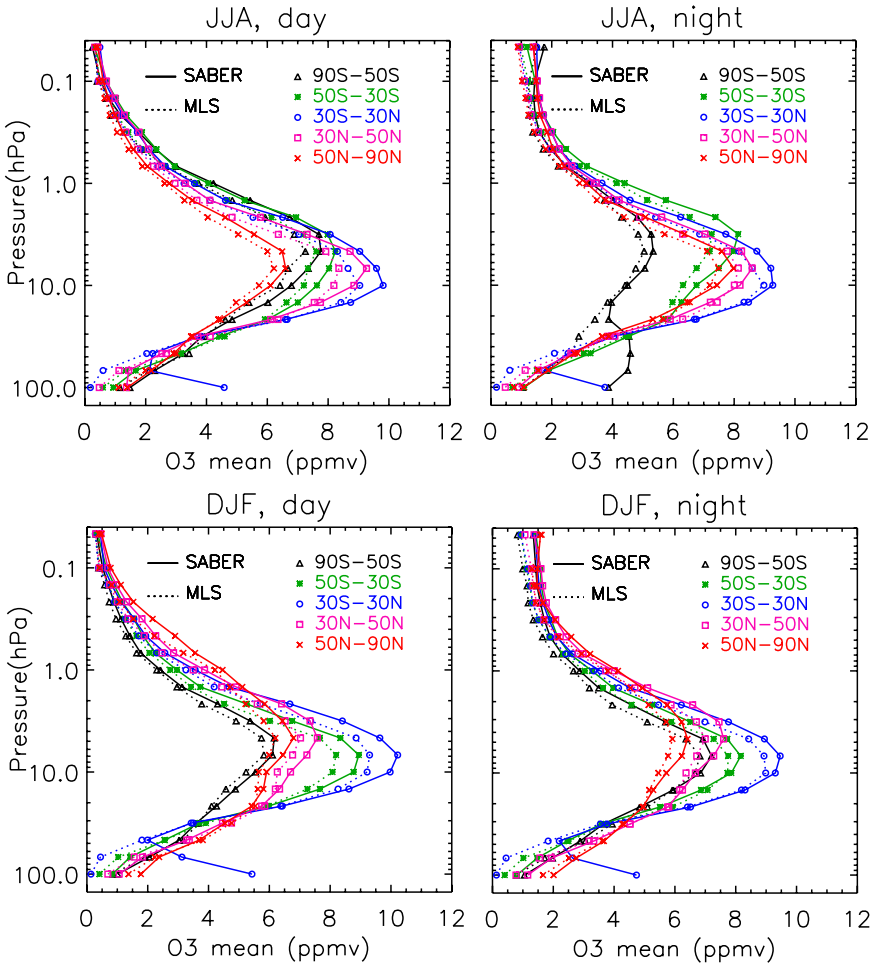

Figure 13. Mean O_3 volume mixing ratio profiles of the day and nighttime comparisons between SABER and MLS v2.2 product for (top) JJA and (bottom) DJF seasons and (left) day and (right) night. All coincidences from 2005 to 2007 are included.

The SAGE (Stratospheric Aerosol and Gas Experiment) II v6.2 O_3 data set was used in this study. We have also performed some comparisons with other well established solar occultation measurements that are not shown here owing to the limited capacity of the paper. For example, SABER versus HALOE (Halogen Occultation Experiment) and SAGE III both have shown mean percent difference of ~17–20% in the stratosphere, which is slightly larger than in the SBUV/2 and MLS results. See *Wang et al.* [2002] and *Wang et al.* [2006] for detailed SAGE II O_3 validation.

[55] The SAGE II instrument operated on board the Earth Radiation Budget Satellite (ERBS), from October 1984 to November 2004. The instrument uses the limb occultation approach, viewing sunset and sunrise in seven different ultraviolet to near infrared channels between approximately 0.2 μm and 1 μm. O_3 profiles are retrieved using the ~0.6 μm band, with a vertical resolution of approximately 1 km. The random error of SAGE II ozone is ~7–10% below 40 km, it increases to ~12% at ~45 km, and rapidly increases to >20% above 60 km. In the SABER and SAGE II O_3 comparisons these values are reduced by a factor of $\sqrt{2}$ owing to the vertical smoothing. The systematic error of SAGE II reaches ~7–8% throughout the stratosphere [*Chu and McCormick*, 1989; *Cunnold et al.*, 1989].

[56] Owing to the limited number of measurements per day all coincidences from year 2002 to 2004 were combined into one ensemble. SABER daytime only comparisons were performed because as was noted, solar occultation measurements do not capture the enhanced O_3 at night.

[57] Figure 16 (left) shows the mean O_3 profiles for SABER and SAGE II. The vertical distribution of the absolute differences is similar to what was observed in comparisons with other measurements. In the middle to upper stratosphere (20–2 hPa) there is a positive bias of ~0.7 ppmv or less. The mean profiles show very good agreement in the lower stratosphere and lower mesosphere. SABER is again biased high in the middle to upper stratosphere. The corresponding percent difference analysis in Figure 16 (right) indicates excellent agreement (~10% or slightly larger) throughout the vertical range 60–0.2 hPa. The largest mean percent difference is still at ~2–3 hPa above the O_3 peak where it gets very close to the combined systematic error. The mean percent difference in the mesosphere in range ~0.2–0.7 hPa is surprisingly small, i.e., ~5–7%, which is unprecedented among all the lower mesospheric comparisons performed above. The standard deviations of the percent differences agree well with the

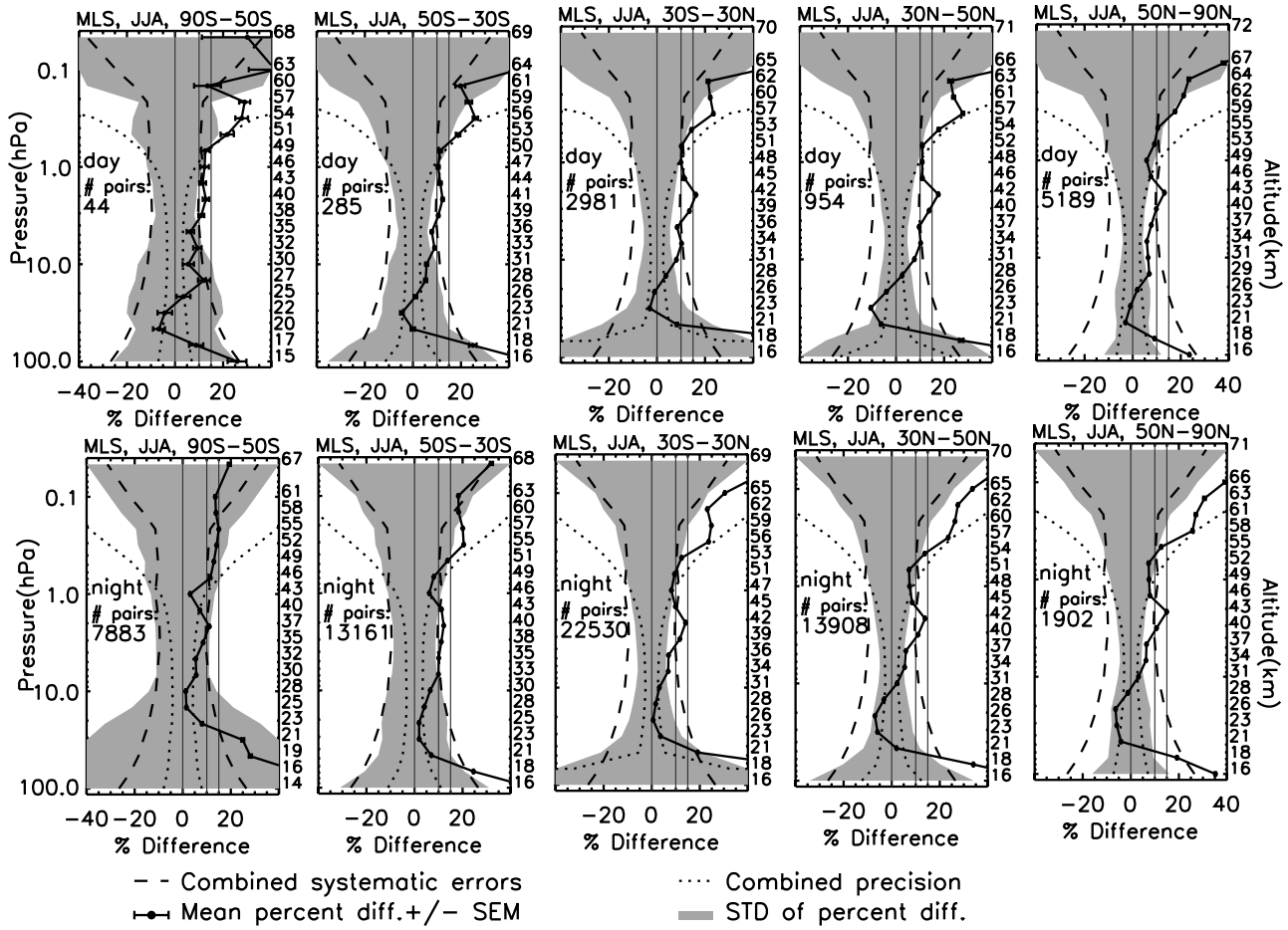

Figure 14. Ozone percent difference statistics and the combined errors for SABER and MLS v2.2 comparisons in JJA season. Altitudes for each panel are indicated on the right-hand *y* axes. (top) Daytime comparisons. (bottom) Nighttime comparisons. Guide lines of 10% and 15% are plotted.

combined random errors except for some discrepancies in the lower stratosphere (>50 hPa).

[58] We next perform a series of comparisons of opportunity using ozonesonde and lidar measurements from the Network for the Detection of Atmospheric Composition Change (NDACC) [*Keckhut and McDermid*, 2004]. Three ECC (electrochemical concentration cell) sonde stations, at Lauder (45°S, 170°E), Hilo (20°N, 155°W), Eureka (80°N, 86°W), and one BM (Brewer Mast) station, Hohenpeissenberg (48°N, 11°E) were chosen for the comparisons. The ECC stations in the NDACC follow a common standard of measurements according to JOSIE (Jülich Ozone Sonde Intercomparison Experiment) report [*Smit and Sträter*, 2004]. Typical ozonesonde precision is ∼5–7%, and the accuracy is ∼3–5%. The vertical resolutions of ECC sonde data vary from 10 m to 0.5 km, depending on the station and sonde type. Figure 17 shows the mean O_3 profiles for SABER and the sondes using data from 2002 to 2006, and Figure 18 shows the corresponding percent differences. In the range ∼22–28 km the mean percent differences remain between ±5%, whereas below 20 km the positive bias increases rapidly downward. The large percent difference below 20 km is mostly due to the low O_3 vmrs, while the absolute difference indicates rather good agreement throughout the entire valid range of ozonesonde measurements except for Hilo, in which the large difference is unequivocally caused by the large SABER O_3 in the equatorial lower stratosphere (see Figure 17). We also noted that the STDs are significantly larger than the combined precision in middle to high latitudes partly owing to the fact that we combined the coincidences in all seasons.

[59] Differential absorption ozone lidar (DIAL) stations from NDACC at Mauna Loa (19°N, 155°W), Table Mountain (34.4°N,117.7°W), OHP (43°N, 5°E), and Ny-Alesund (78.9°N,12°E) were also used to make comparisons (Figures 19 and 20). The useful range of DIAL ozone is up to ∼45 km. There are more coincidences than with the ECC sondes because the lidar measurements are taken daily. The typical vertical resolution of lidar measured ozone is ∼0.5–3 km. For each lidar O_3 profile the corresponding error profile is provided. We used the RMS of single profile errors as the total lidar error estimate. From the O_3 mean profiles we see overall good agreement between SABER and lidar O_3. The maximum absolute difference can reach ∼1 ppmv. The mean percent differences stay within ∼10% in most cases except for the upper stratosphere (<1 hPa) where the lidar measurements significantly drift toward lower O_3 vmrs. We can see that in the SABER and lidar

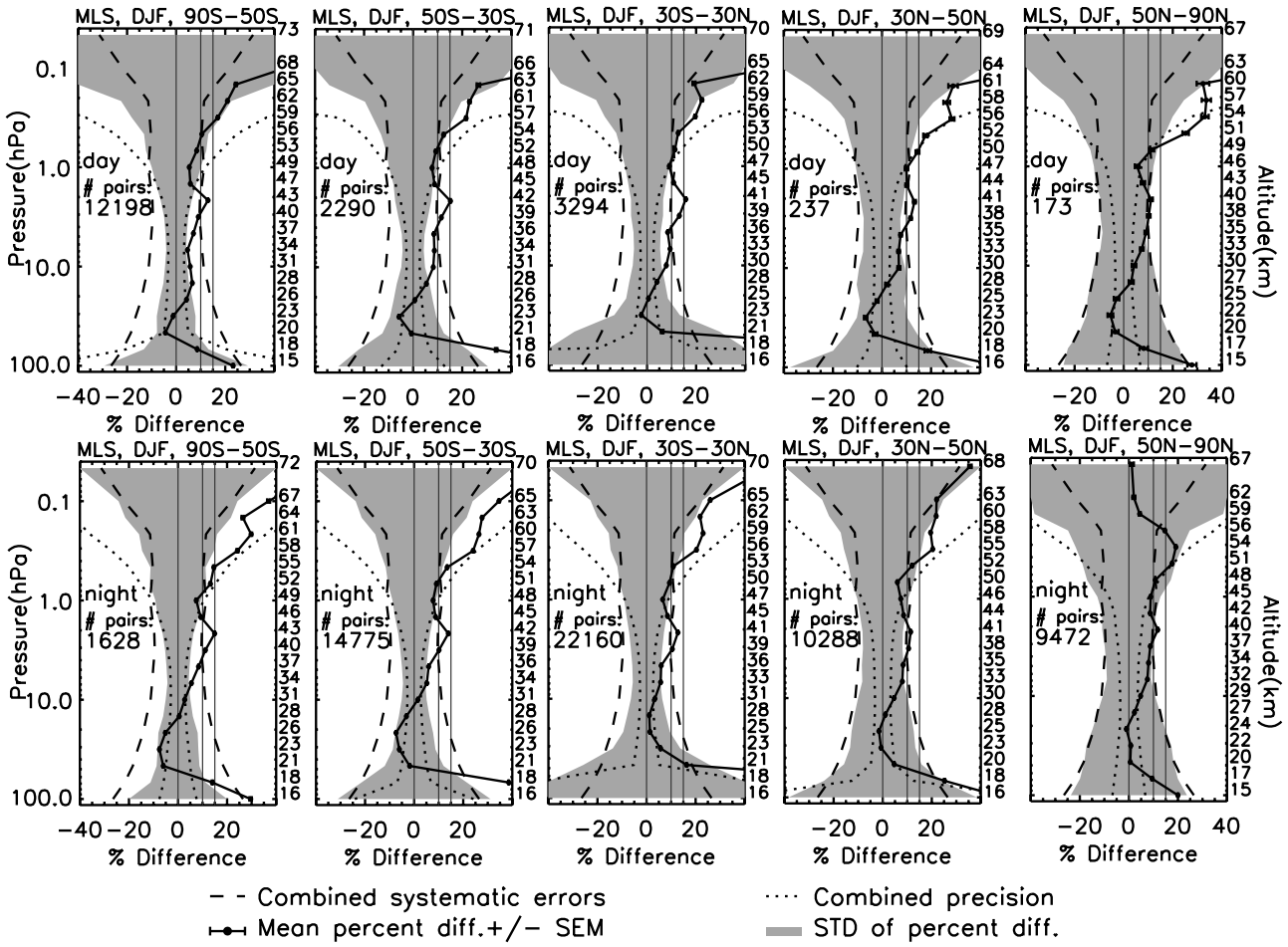

Figure 15. Same as Figure 14 except for DJF season.

O_3 comparisons the RMS difference is dominated by the standard deviation (8–10% or larger), indicating also large random variability.

8. Detection of Abnormal Profiles

[60] Data screening is a necessary step for proper data use in order to rule out unusually large or negative O_3 values. These indices are not available for SABER v1.07 data. We used a probability method (see section 3.4) in this paper to give a warning sign of possible anomalous profiles. This approach reveals the exact latitude bin (10 degree) and altitude range where the anomalous values occur. After narrowing the time and space of these occurrences the responsible profiles can be traced quickly. A key point of this approach is that the differences between individual coincident pairs must follow a Gaussian distribution under the condition that there are no controlling factors that are solely present in one of the two data sets. As a result some large SABER O_3 values will lead to deviation of the coincidence frequency from a Gaussian form. Other types of anomaly could also occur, for example, in the SABER and MIPAS comparisons we will see that O_3 day and night differences in the mesosphere often lead to large deviation of the coincidence frequency from a Gaussian form due to the fact that rapid O_3 change can occur within the given time coincident box of 2 h.

[61] Figure 21 displays a map of probability deviation for SABER and SBUV/2 comparisons in SON. In this map, statistics were computed in every 10-degree latitude bin. Contours with value of 0.3 were emphasized to divide small

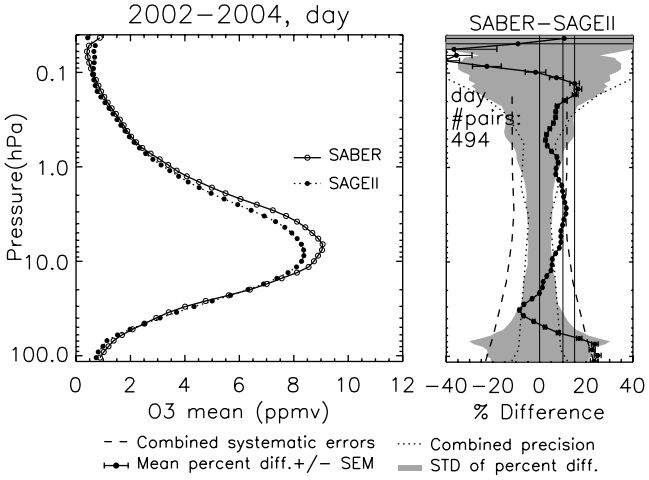

Figure 16. SABER O_3 and SAGE II v2.2 O_3 comparisons. All coincidences in 2002–2004 are included. Daytime-only SABER profiles are used. (left) Mean O_3 volume mixing ratio profiles for SABER and SAGE II. (right) Percent difference statistics and the combined errors.

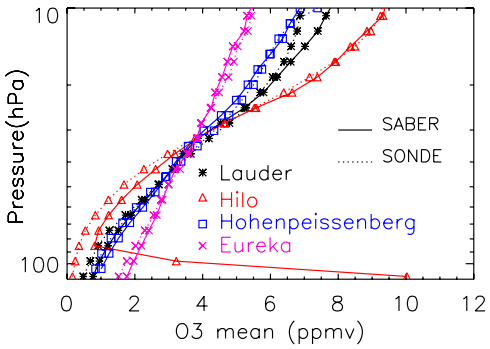

Figure 17. Mean O_3 volume mixing ratio profiles for SABER and ozonesonde comparisons. Four stations, Lauder (45°S, 170°E), Hilo (20°N, 155°W), Eureka (80°N, 86°W), and Hohenpeissenberg (48°N, 11°E), are selected, and all coincidences from 2002 to 2006 are used.

to large deviations in a relative sense. Figure 21 shows that in most regions there is fairly small deviation (<0.3), implying excellent Gaussian fittings, while in the southern hemisphere polar region it is significantly worse. The 80°N–90°N latitude bin also shows "noisier" and larger values but the small sample number (e.g., 19) makes the statistics unreliable. No serious attention should be given to deviations in such regions.

[62] The coincidence frequency versus the O_3 percent difference and the corresponding Gaussian fitting at different pressure levels are displayed in Figure 22. In the upper stratosphere (i.e., 5.01 hPa and 0.89 hPa) the Gaussian fittings are near-perfect while at 34.67 hPa a significant deviation was observed owing to the fact that some coincidences show either large negative or large positive differences. The bottom panels presented two pairs of coincident profiles that have caused such deviation. It is clearly shown that the high SABER O_3 in the lower stratosphere polar region is the cause of the deviation in the positive direction, while in an opposite case SBUV/2 O_3 seems much larger than SABER O_3 although no anomalous peak appeared in the SBUV/2 profile. Both types of anomalies have occurred for a certain fraction of the data and therefore caused the deviation shown in the top panel. The gray lines are the 99% guide line for the Gaussian, and we only used data points that fall between the gray lines to compute the mean percent differences. Apparently sometimes large positive or negative differences could be included in the mean difference calculation.

[63] A similar probability map for MIPAS JJA nighttime is shown in Figure 23 to expand the examination. It again shows large deviation in the southern polar region lower stratosphere. An investigation of this region (not presented) indicated that large SABER O_3 (similar to what is shown in Figure 22) was still the cause of this probability deviation. Polar stratospheric clouds could be a cause of this occurrence but in the previous analysis September is almost the spring time in the southern hemisphere. This problem should be carefully examined to interpret the results properly. The equatorial region also presents large deviations. The SBUV/2 comparisons did not fully reveal this because its vertical range starts at higher altitudes (>20 km). The deviation in the equatorial region is also caused by the same type of large SABER O_3. Normal clouds are very likely the cause of large SABER O_3 in the lower stratosphere and below.

[64] The probability deviation in the mesosphere has a very different cause from those discussed above. Figure 24 shows the coincidence frequency versus the O_3 percent difference, and the O_3 profiles, for 70°S–60°S latitude bin in JJA at night. We can see that at 1.45 hPa and 0.48 hPa the Gaussian fittings are near-perfect but at 0.1 hPa large deviations occurred owing to a smaller second peak that appeared in the range of large positive percent differences. Figure 24 (bottom) shows examples of coincident profiles that caused such deviations. It is interesting to note that MIPAS and SABER O_3 vmrs exhibit drastically different day and night behavior. When the detailed time and longitude differences are noted, it can be seen that the MIPAS occurrence was indeed closer to daytime. Both data sets could be reasonable in this circumstance since we have seen

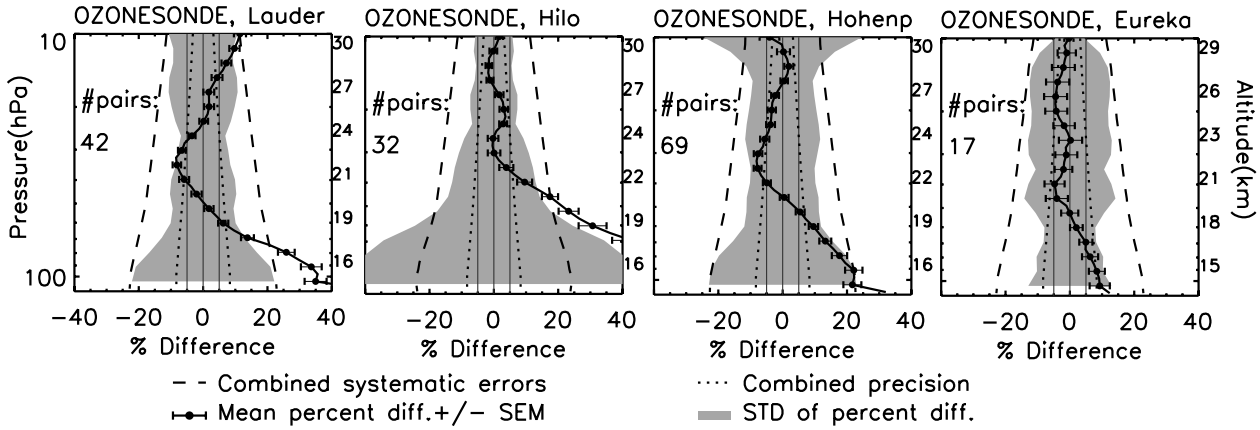

Figure 18. Ozone percent difference statistics and the combined errors for SABER and ozonesonde comparisons for the four stations selected in Figure 17. Guide lines of ±5% are provided. Altitudes for each panel are indicated on the right-hand *y* axes.

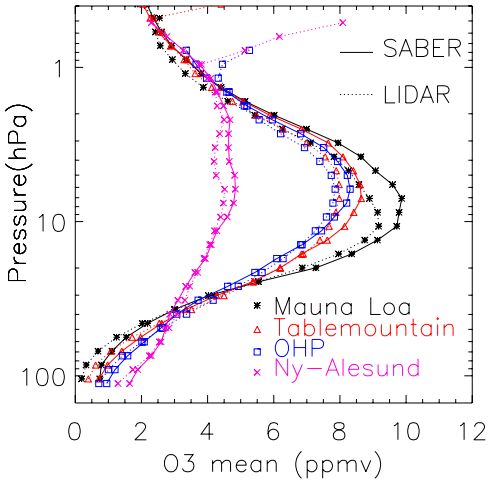

Figure 19. Mean O_3 volume mixing ratio profiles for SABER v1.07 and DIAL lidar comparisons. Four stations, Mauna Loa (19°N, 155°W), Table Mountain (34.4°N, 117.7°W), OHP (43°N, 5°E), and Ny-Alesund (78.9°N, 12°E), are chosen, and all coincidences from 2002 to 2006 are used.

the "plateau" change between day and night O_3, which suggests that the O_3 change is rapid during twilight.

9. Mismatch Statistics

[65] As discussed in a former section the coincidence criteria given in this study are 10 degrees in longitude, 2.0 degrees in latitude, and 2 h in time. Such flexibility is allowed not only because perfect coincidences are unlikely to occur between different instruments, but also because we rely on the assumption that O_3 varies only modestly within the defined time and spatial ranges. We believe the criteria used here are reasonable but still the boundary blurs regarding whether they are the best choice and to what degree the O_3 differences are caused by such mismatches.

[66] Impact of mismatches on the data differences has been discussed and quantified by *Cortesi et al.* [2007] using a data assimilation technique. For SABER ozone, we tested the correlation between the ozone differences and the mismatches by examining their statistics prior to considering any further approaches.

[67] Figure 25 presents scatterplots between the O_3 absolute difference versus time difference, latitude difference, and longitude difference, respectively. Figure 25 (left) and Figure 25 (middle) show SABER-SBUV/2 and SABER-MIPAS, respectively, in 30°S–30°N and at 40 km. We first note that in both MIPAS and SBUV/2 the differences in longitude (Δlon) and latitude (Δlat) are mostly symmetric about zero with only slight departures. But in time (Δtime) strong asymmetries are noted in both comparisons. In other words, there are more pairs with Δtime > 0. However, in both SBUV/2 and MIPAS results we can see that the asymmetry of the Δtime distribution has a negligible impact on the O_3 mean differences in 30°S–30°N. The consistently larger O_3 differences in 30°S–30°N SBUV/2 comparisons (1.0 ppmv versus 0.6 ppmv in MIPAS) are caused by something other than time or spatial mismatch. Figure 25 (right) shows the case for SBUV/2 JJA comparisons in 50°N–90°N. We have known from the discussion above that polar summer is the region that shows the best agreement in SBUV/2 comparisons, but we clearly see that the bias weakly increases as Δtime increases further from zero, which could have made the bias increased, say, by a few percent. This later case was presented just to indicate that mismatch could impact the biases, but in most cases, given a reasonably tight coincidence box and large number of coincidences, mismatch in space or time did not prove to be the main cause of the biases.

10. Summary and Conclusions

[68] The purpose of this study is to assess the quality of SABER v1.07 O3_96 data in the altitude range 15–70 km (~115–0.04 hPa). On the basis of measurement repeatabil-

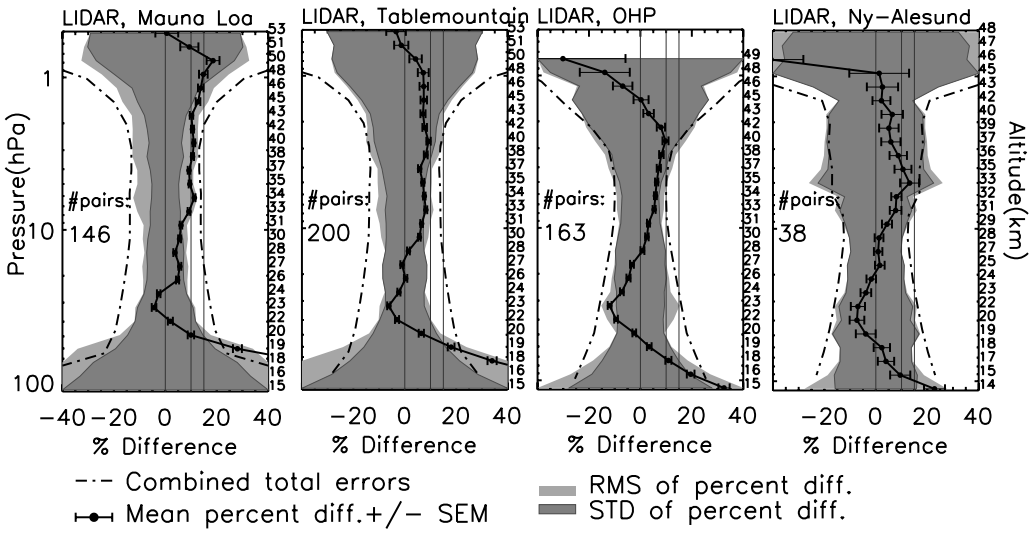

Figure 20. Ozone percent difference statistics and the combined errors for SABER and DIAL lidar comparisons for the same stations as shown in Figure 19. Altitudes for each panel are indicated on the right-hand *y* axes.

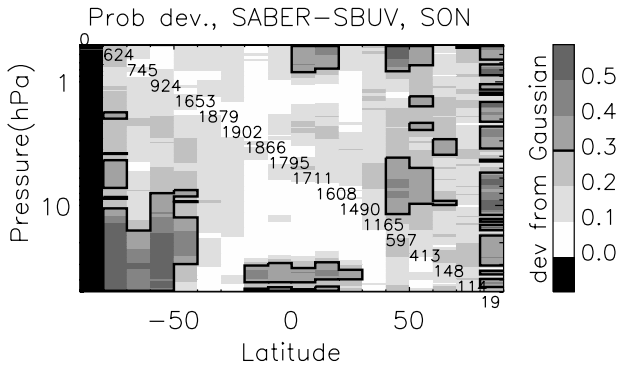

Figure 21. Latitude-pressure cross section of probability deviation (defined in the text) from Gaussian for SABER and SBUV/2 comparisons in SON season. Value 0.3 is shown as thick dark line to divide relatively small versus large values. Number of coincidences in each 10-degree latitude bin is indicated.

ity studies, the SABER O3_96 precision is ~1–2% in the ~50- to 0.4-hPa (~20–55 km) range and it increases rapidly in the lower stratosphere. The SABER O3_96 estimated total precision based on retrieval simulations of the primary error sources in the 100- to 0.4-hPa range agrees well with the precision from the repeatability test. SABER precision is generally very high except for lower stratosphere. Estimated SABER systematic errors vary between 23% and 9% from the lower to upper stratosphere, and they are 1–2% higher in the middle to upper stratosphere than the systematic errors in most other correlative data sets.

[69] A large number of comparisons were performed between SABER O_3 and a series of large satellite data sets, including SBUV/2, MIPAS, MLS, and SAGE II. Comparisons were also carried out with O_3 measurements from several ozonesonde and lidar stations. Coincident pairs of O_3 profiles were selected using the criteria of 10 degrees in longitude, 2 degrees in latitude, and 2 h in time. Statistics of O_3 percent differences were examined for different seasons but coincidences for different years were combined.

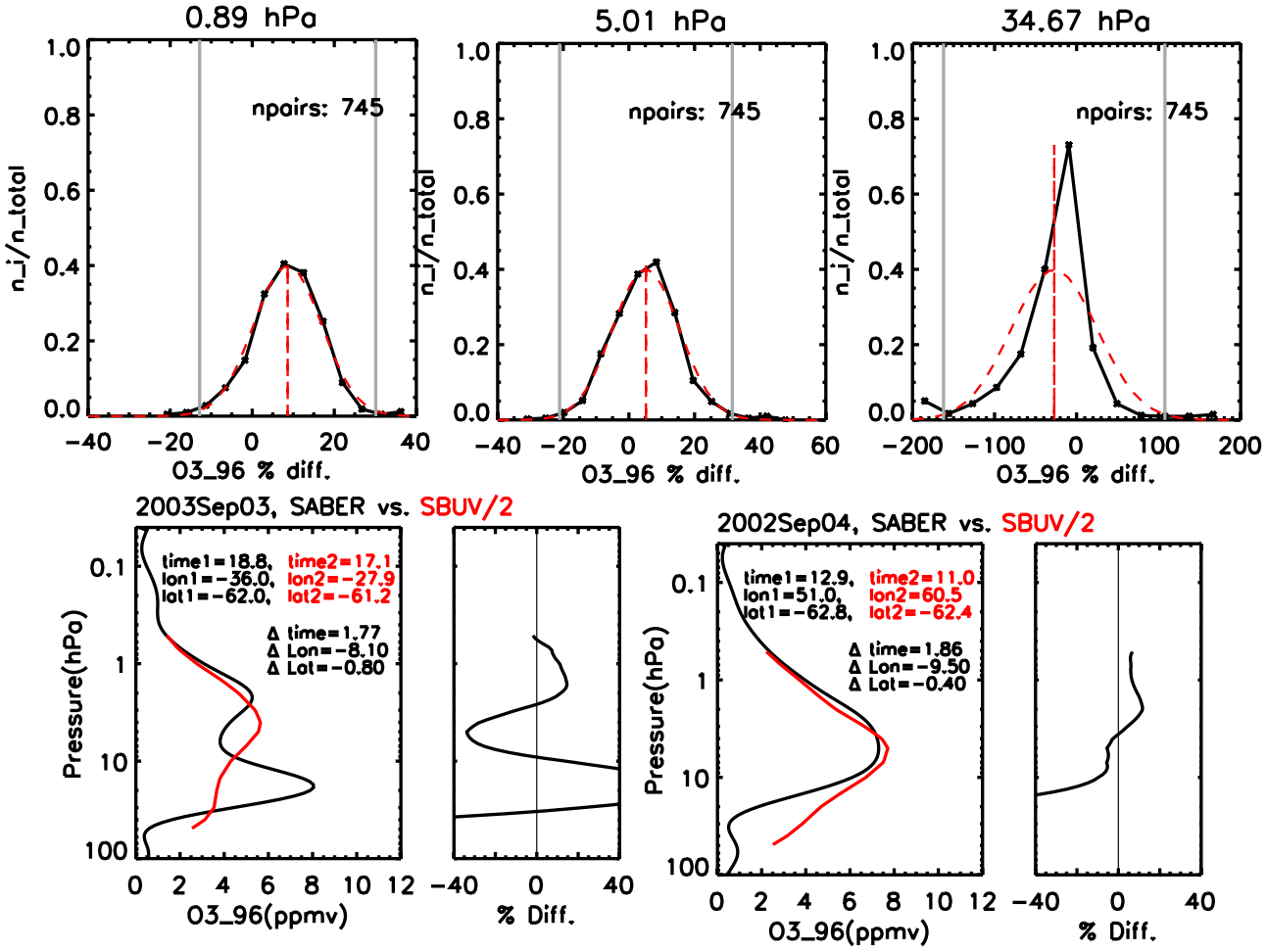

Figure 22. Demonstration of how anomalous pairs of profiles cause the large deviation from Gaussian. Latitude bin 70°S–60°S (shown in large deviation from Gaussian in Figure 21) is chosen to perform the analysis. (top) Examples of good and poor fitting of the Gaussian distribution (dashed line) to the coincidence frequency (solid line with symbols) versus O_3 percent difference. The gray lines are 99% guide lines of the Gaussian distribution. (bottom) Two pairs of poorly agreed profiles.

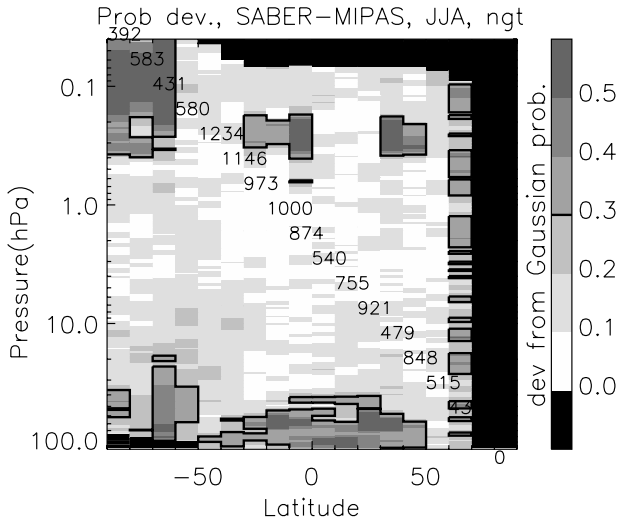

Figure 23. Latitude-pressure cross section of probability deviation from Gaussian for SABER and MIPAS comparisons in JJA nighttime.

[70] SABER O_3 is biased high in the middle to upper stratosphere and throughout the lower mesosphere in all comparisons. The bias in the stratosphere varies from 5% to 17%, and the largest values are in equatorial and middle latitudes upper stratosphere ~30–50 km. The fact that this bias exceeds the combined estimated systematic error by ~5–6% indicates that there might be either an underestimate of SABER individual systematic errors or unidentified error sources in this vertical range. SABER versus SBUV/2 and MLS O_3 comparisons show similar results in the daytime stratosphere. The comparisons between SABER and MIPAS O_3 show overall much better agreement than with the other two data sets. The positive bias in the stratosphere in MIPAS results exceeds 10–12% only occasionally. SABER and MIPAS O_3 nighttime comparisons show even better agreement (by a few percent) than their daytime counterparts. In the lower mesosphere SABER and MIPAS nighttime comparisons show relatively good agreement. Daytime mesospheric percent agreement is generally poorer owing to the lower O_3 vmr. SABER and SAGE II O_3 comparisons in the lower mesosphere, however, show excellent agreement, with a bias of ~5–7%.

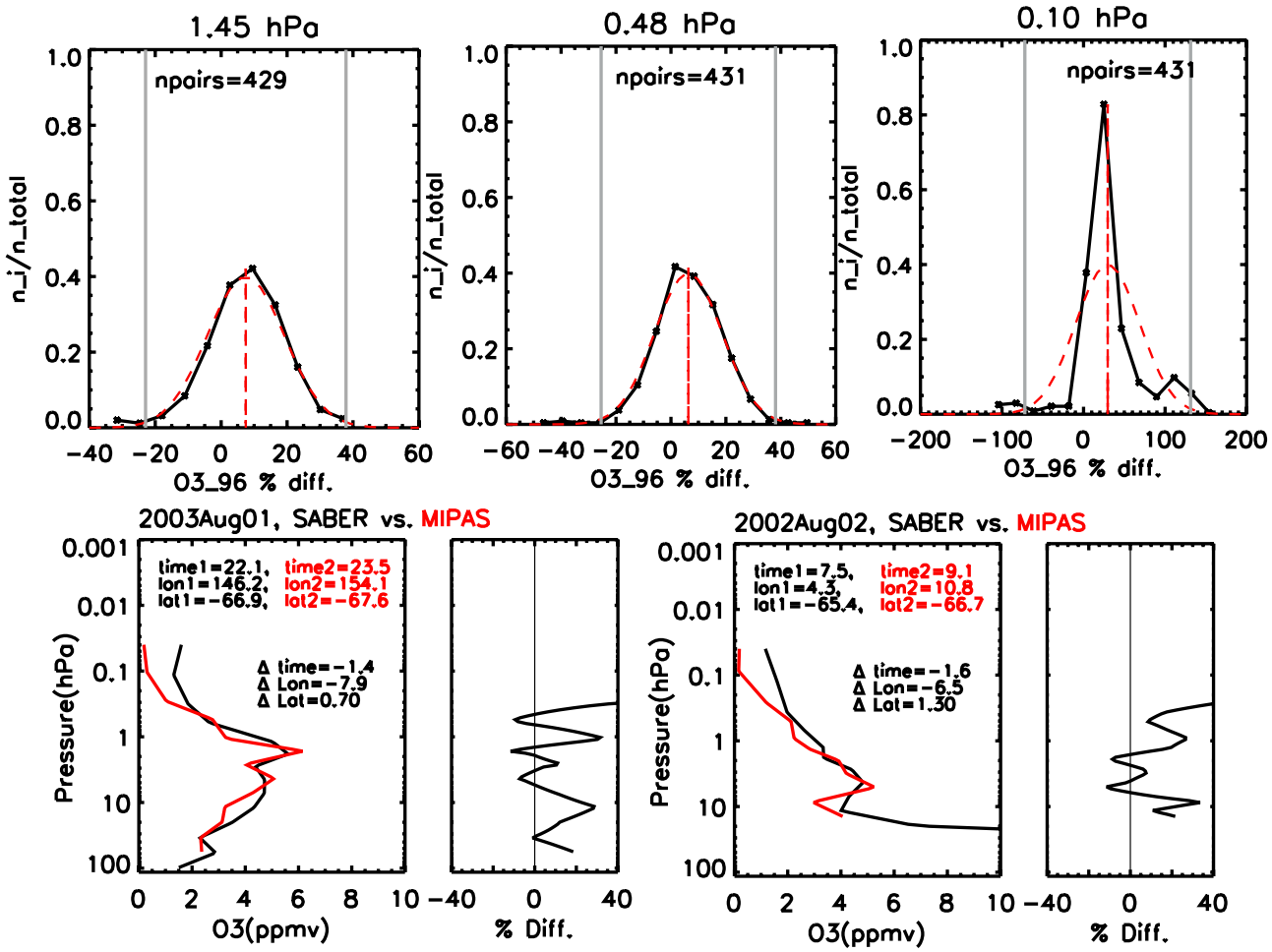

Figure 24. Demonstration plots similar to the SBUV/2 case as in Figure 22 except for MIPAS. Latitude bin 70°S–60°S is chosen to perform the analysis but the focus is on the lower mesosphere. A few pairs of profiles show drastic day and night contrast in O_3 volume mixing ratios, and in most such cases MIPAS profiles present daytime behavior.

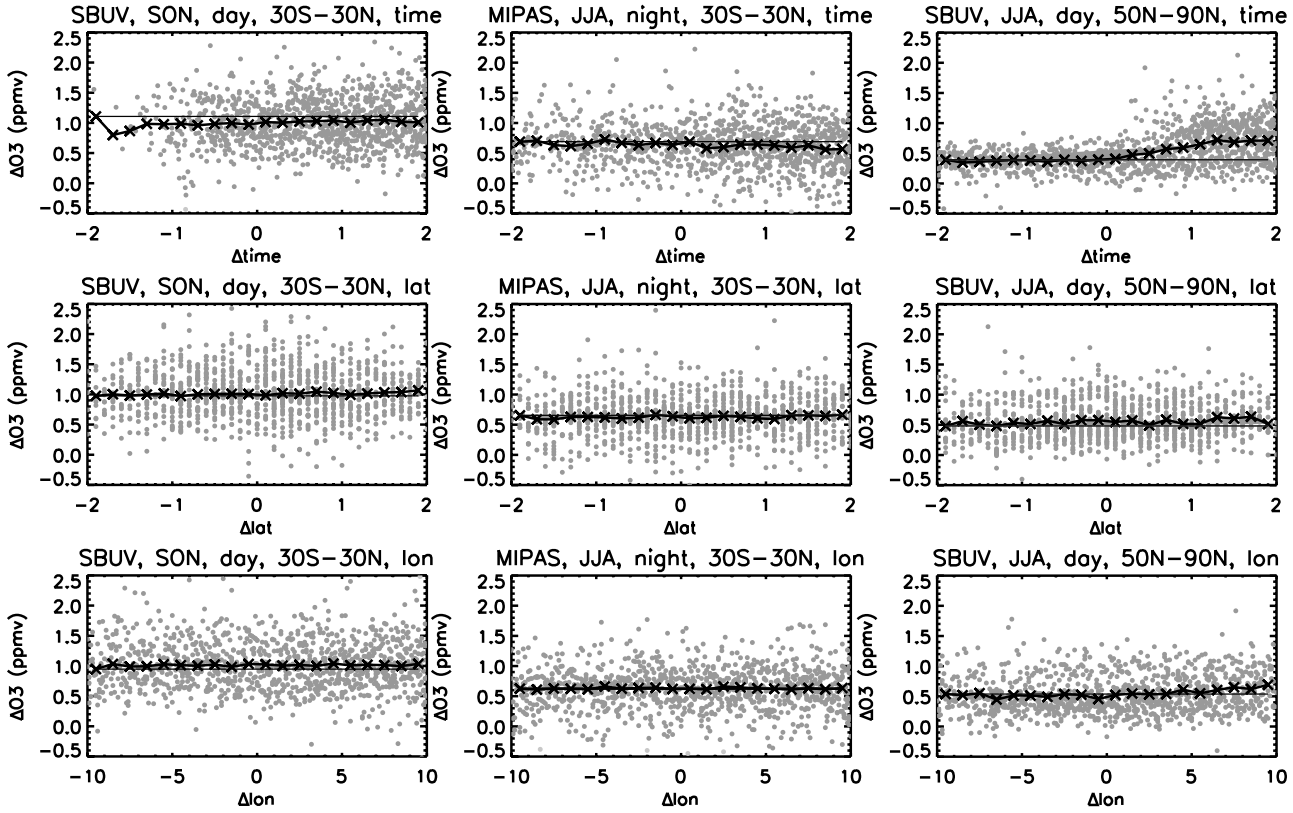

Figure 25. Impact of spatial and time mismatch upon the O_3 absolute differences. The gray dots are scatterpoints of the coincidences, and the black crosses represent the mean absolute differences in the individual bins of Δtime, Δlat, and Δlon. The bins are spaced by the intervals between adjacent crosses. (left) SBUV comparisons in SON and in latitude band 30°S–30°N. The coincidences at 40-km surface are examined. Other altitude levels are nearly identical. (middle) Same as left except for MIPAS JJA nighttime comparisons. (right) SBUV/2 JJA comparisons in 50°N–90°N. The thin black horizontal lines are guide lines with values of the first crosses in each panel.

[71] A probability approach was used as an effective tool to detect anomalous profiles. Anomalously large SABER O_3 values mostly occur in the southern polar stratosphere below 30 km and the equatorial region. Caution should be used when selecting profiles in those regions.

[72] The biases shown in all the comparisons are very likely a reflection of a true systematic bias in SABER O3_96. The positive biases in the upper stratosphere to lower mesosphere are correlated with the negative temperature biases in the same vertical range [*Remsberg et al.*, 2008]. By improving the accuracy in temperature retrieval we can remove part of the high O_3 biases. An error in retrieved pressure is also an important contributing factor that leads to biases in both temperature and O3_96. Work is underway to better understand the biases, to improve the algorithm and therefore lessen the systematic biases. In the meantime, knowing these percent differences and their distributions provides a helpful guide for using SABER data in scientific applications.

[73] **Acknowledgments.** This work was accomplished in the Center for Atmospheric Sciences (CAS), Hampton University, Hampton, Virginia. We are grateful to the SABER retrieval team, including scientists from GATS, Inc, NASA Langley Research Center, NASA Goddard Space Flight Center, and IAA, Spain, for their hard work and invaluable support. We acknowledge scientists from the SBUV team who mailed the CD to us in a timely manner for our immediate use. We acknowledge the European Space Agency for approving our request to use MIPAS reanalysis data, and also acknowledge the MLS team from JPL who made MLS v1.5 and v2.2 data available online to download and also provided the subroutines. We also acknowledge the SAGE II team who made their data available and furthermore appreciate John Anderson from CAS, who reprocessed the data for our convenient use. We last acknowledge scientists who have organized and maintained the NDACC website for many years and made the ozonesonde and lidar O_3 available. This work is supported under NASA contract NAG 5–11409.

References

Bhartia, P. K., R. D. McPeters, C. L. Mateer, L. E. Flynn, and C. G. Wellemeyer (1996), Algorithms for the estimation of vertical profiles from the backscattered ultraviolet technique, *J. Geophys. Res.*, *101*, 18,793–18,806, doi:10.1029/96JD01165.

Chu, W. P., and M. P. McCormick (1989), SAGE II inversion algorithm, *J. Geophys. Res.*, *94*, 8339–8351, doi:10.1029/JD094iD06p08339.

Cortesi, U., et al. (2007), Geophysical validation of MIPAS-ENVISAT operational ozone data, *Atmos. Chem. Phys.*, *7*, 4807–4867.

Cunnold, D. M., W. P. Chu, R. A. Barnes, M. P. McCormick, and R. E. Veiga (1989), Validation of SAGE II ozone measurements, *J. Geophys. Res.*, *94*, 8447–8460, doi:10.1029/JD094iD06p08447.

Dakermanji, G., M. Butler, P. U. Carlsson, and D. Temkin (1997), The Thermosphere, Ionosphere, Mesosphere Energetics And Dynamics (TIMED) spacecraft power system, paper presented at Energy Conversion Engineering Conference: 32nd Intersociety, Am. Int. Aeronaut. and Astronaut., Reston, Va.

Dials, M. A., J. C. Gille, J. J. Barnett, and J. G. Whitney (1998), Description of the High Resolution Dynamics Limb Sounder (HIRDLS) instrument, *Proc. SPIE Int. Soc. Opt. Eng.*, *3437*, 84–91, doi:10.1117/12.331309.

Fischer, H., et al. (2000), ENVISAT, MIPAS: An instrument for atmospheric chemistry and climate research*ESA SP-1229*, Eur. Space Agency, Nordwijk, Netherlands.

Froidevaux, L., et al. (2008), Validation of Aura Microwave Limb Sounder stratospheric ozone measurements, *J. Geophys. Res.*, *113*, D15S20, doi:10.1029/2007JD008771.

Gille, G. C., and J. M. Russell III (1984), The Limb Infrared Monitor of the Stratosphere: Experiment description, performance, and results, *J. Geophys. Res.*, *89*, 5125–5140, doi:10.1029/JD089iD04p05125.

Gordley, L. L., and J. M. Russell III (1981), Rapid inversion of limb radiance data using an emissivity growth approximation, *Appl. Opt.*, *20*(5), 807–813, doi:10.1364/AO.20.000807.

Keckhut, P., and S. McDermid (2004), Review of ozone and temperature lidar validations performed within the framework of the Network for the Detection of Stratospheric Change, *J. Environ. Monit.*, *6*, 721–733, doi:10.1039/b404256e.

Marshall, B. T., L. L. Gordley, and D. A. Chu (1994), BANDPAK algorithms for modeling broadband transmission and radiance, *J. Quant. Spectrosc. Radiat. Transfer*, *52*, 581–599, doi:10.1016/0022-4073(94)90026-4.

Mlynczak, M. G., and R. Drayson (1990a), Calculation of infrared limb emission by ozone in the terrestrial middle atmosphere: 1. Source functions, *J. Geophys. Res.*, *95*, 16,497–16,511, doi:10.1029/JD095iD10p16497.

Mlynczak, M. G., and R. Drayson (1990b), Calculation of infrared limb emission by ozone in the terrestrial middle atmosphere: 2. Emission calculations, *J. Geophys. Res.*, *95*, 16,513–16,521, doi:10.1029/JD095iD10p16513.

Mlynczak, M. G., D. S. Olander, and M. Lopez-Puertas (1994), Rapid computation of spectrally integrated nonlocal thermodynamic equilibrium limb emission, *J. Geophys. Res.*, *99*, 25,761–25,772, doi:10.1029/94JD02397.

Nazaryan, H., M. P. McCormick, and J. M. Russell III (2007), Comparative analysis of SBUV/2 and HALOE ozone profiles and trends, *J. Geophys. Res.*, *112*, D10304, doi:10.1029/2006JD007367.

Randall, C. E., et al. (2005), Stratospheric effects of energetic particle precipitation in 2003–2004, *Geophys. Res. Lett.*, *32*, L05802, doi:10.1029/2004GL022003.

Randall, C. E., V. L. Harvey, C. S. Singleton, P. F. Bernath, C. D. Boone, and J. U. Kozyra (2006), Enhanced NO_x in 2006 linked to strong upper stratospheric Arctic vortex, *Geophys. Res. Lett.*, *33*, L18811, doi:10.1029/2006GL027160.

Raspollini, P., et al. (2006), MIPAS level 2 operational analysis, *Atmos. Chem. Phys.*, *6*, 5605–5630.

Remsberg, E. E., G. Lingenfelser, M. Natarajan, L. L. Gordley, B. T. Marshall, and E. Thompson (2007), On the quality of the Nimbus 7 LIMS version 6 ozone for studies of the middle atmosphere, *J. Quant. Spectrosc. Radiat. Transfer*, *105*, 492–518, doi:10.1016/j.jqsrt.2006.12.005.

Remsberg, E. E., et al. (2008), Assessment of the quality of the Version 1.07 temperature versus pressure profiles of the middle atmosphere from TIMED/SABER, *J. Geophys. Res.*, *113*, D17101, doi:10.1029/2008JD010013.

Ricaud, P., J. de La Noë, B. J. Connor, L. Froidevaux, J. W. Waters, R. S. Harwood, I. A. MacKenzie, and G. E. Peckhams (1996), Diurnal variability of mesospheric ozone as measured by the UARS microwave limb sounder instrument: Theoretical and ground-based validations, *J. Geophys. Res.*, *101*, 10,077–10,089, doi:10.1029/95JD02841.

Rothman, L. S., et al. (2003), The HITRAN molecular spectroscopic database: Edition of 2000 including updates through 2001, *J. Quant. Spectrosc. Radiat. Transfer*, *82*, 5–44, doi:10.1016/S0022-4073(03)00146-8.

Russell, J. M., III, and S. R. Drayson (1972), The inference of atmospheric ozone using satellite horizon measurements in the 1042 cm^{-1} band, *J. Atmos. Sci.*, *29*, 376–390, doi:10.1175/1520-0469(1972)029<0376:TIOAOU>2.0.CO;2.

Russell, J. M., III, et al. (1996), Validation of hydrogen chloride measurements made by the Halogen Occultation Experiment from the UARS platform, *J. Geophys. Res.*, *101*, 10,151–10,162, doi:10.1029/95JD01696.

Russell, J. M., III, M. G. Mlynczak, L. L. Gordley, J. J. Larry Tansock, and R. Esplin (1999), Overview of the SABER experiment and preliminary calibration results, *Proc. SPIE Int. Soc. Opt. Eng.*, *3756*, 277–288.

Seppälä, A., P. T. Verronen, E. Kyrölä, S. Hassinen, L. Backman, A. Hauchecorne, J. L. Bertaux, and D. Fussen (2004), Solar proton events of October–November 2003: Ozone depletion in the Northern Hemisphere polar winter as seen by GOMOS/Envisat, *Geophys. Res. Lett.*, *31*, L19107, doi:10.1029/2004GL021042.

Smit, H. G. J., and W. Sträter (2004), Jülich Ozone Sonde Intercomparison 2000 (JOSIE), *WMO GAW TD N.1225*, World Meteorol. Org., Geneva.

Smith, M. A. H., and L. L. Gordley (1983), Sensitivity of ozone retrievals in limb-viewing experiments to errors in line-width parameters, *J. Quant. Spectrosc. Radiat. Transfer*, *29*, 413–418.

Tansock, J. J., J. M. Russell III, M. G. Mlynczak, L. L. Gordley, C. Brown, G. Paxton, and P. McMichaels (2006), An update of sounding of the atmosphere using broadband emission radiometry (SABER) calibration, *Proc. SPIE Int. Soc. Opt. Eng.*, *6297*, 6297OV, doi:10.1117/12.692857.

von Clarmann, T. (2006), Validation of remotely sensed profiles of atmospheric state variables: Strategies and terminology, *Atmos. Chem. Phys.*, *6*, 4311–4320.

Wang, H.-J., D. M. Cunnold, L. W. Thomason, Z. M. Zawodny, and G. E. Bodeker (2002), Assessment of SAGE version 6.1 ozone data quality, *J. Geophys. Res.*, *107*(D23), 4691, doi:10.1029/2002JD002418.

Wang, P. H., et al. (2006), Ozone variability in the midlatitude upper troposphere and lower stratosphere diagnosed from a monthly SAGE II climatology relative to the troposphere, *J. Geophys. Res.*, *111*, D21304, doi:10.1029/2005JD006108.

Waters, J. W., et al. (2006), The Earth Observing System Microwave Limb Sounder (EOS MLS) on the Aura Satellite, *IEEE Trans. Geosci. Remote Sens.*, *44*, 1075–1092.

Wild, J. D., et al. (2005), Validation and use of SBUV/2 ozone profiles for operational and climate monitoring purposes, *Geophys. Res. Abstr.*, *7*, 03735.

Yokota, T., et al. (2002), Improved Limb Atmospheric Spectrometer (ILAS) data retrieval algorithm for Version 5.20 gas profile products, *J. Geophys. Res.*, *107*(D24), 8216, doi:10.1029/2001JD000628.

L. L. Gordley and B. T. Marshall, GATS, Inc., Newport News, VA 23606, USA.

M. López-Puertas, Instituto de Astrofísica de Andalucíca, CSIC, E-18008 Grenada, Spain.

M. G. Mlynczak and E. E. Remsberg, NASA Langley Research Center, Hampton, VA 23681, USA.

P. P. Rong and J. M. Russell III, Hampton University, Hampton, VA 23668, USA.